

# HST/ACS colour-magnitude diagrams of M31 globular clusters <sup>★</sup>

S. Perina<sup>1</sup>, L. Federici<sup>2</sup>, M. Bellazzini<sup>2</sup>, C. Cacciari<sup>2</sup>, F. Fusi Pecci<sup>2</sup>, and S. Galletti<sup>2</sup>

<sup>1</sup> Università di Bologna, Dipartimento di Astronomia Via Ranzani 1, 40127 Bologna, Italy  
e-mail: sibilla.perina@unibo.it

<sup>2</sup> INAF - Osservatorio Astronomico di Bologna, Via Ranzani 1, 40127 Bologna, Italy  
e-mail: luciana.federici@oabo.inaf.it, michele.bellazzini@oabo.inaf.it,  
flavio.fusipecchi@oabo.inaf.it, carla.cacciari@oabo.inaf.it, silvia.galletti@oabo.inaf.it

Received May 28, 2009; accepted September 23, 2009

## ABSTRACT

**Aims.** With the aim of increasing the sample of M31 clusters for which a colour-magnitude diagram is available, we searched the HST archive for ACS images containing objects included in the Revised Bologna Catalogue of M31 globular clusters <sup>\*\*</sup>.

**Methods.** Sixty-three such objects were found. We used the ACS images to confirm or revise their classification and were able to obtain useful CMDs for 11 old globular clusters and 6 luminous young clusters. We obtained simultaneous estimates of the distance, reddening, and metallicity of old clusters by comparing their observed field-decontaminated CMDs with a grid of template clusters of the Milky Way. We estimated the age of the young clusters by fitting with theoretical isochrones.

**Results.** For the old clusters, we found metallicities in the range  $-0.4 \leq [\text{Fe}/\text{H}] \leq -1.9$ . The individual estimates generally agree with existing spectroscopic estimates. At least four of them display a clear blue horizontal branch, indicating ages  $\geq 10$  Gyr. All six candidate young clusters are found to have ages  $< 1$  Gyr. The photometry of the clusters is made publicly available through a dedicated web page.

**Conclusions.** With the present work the total number of M31 GCs with reliable optical CMD increases from 35 to 44 for the old clusters, and from 7 to 11 for the young ones. The old clusters show similar characteristics to those of the MW. We discuss the case of the cluster B407, with a metallicity  $[\text{Fe}/\text{H}] \approx -0.6$  and located at a large projected distance from the centre of M31 ( $R_p = 19.8$  kpc) and from the major axis of the galaxy ( $Y = 11.3$  kpc). Metal-rich globulars at large galactocentric distances are rare both in M31 and in the Milky Way. B407, in addition, has a velocity in stark contrast with the rotation pattern shared by the bulk of M31 clusters of similar metallicity. This, along with other empirical evidence, supports the hypothesis that the cluster (together with B403) is physically associated with a substructure in the halo of M31 that has been interpreted as the relic of a merging event.

**Key words.** Galaxies:individual:M31 – Galaxies:star clusters – Catalog — (Galaxies:)Local Group

## 1. Introduction

Over the past  $\sim 20$  years, the globular cluster (GC) system of M31 has been the subject of intensive study both from the ground and from space-borne observatories (see Rich et al. 2005; Galletti et al. 2004 - hereafter G04, 2006a, 2007; Huxor et al. 2008; Lee et al. 2008 and Caldwell et al. 2009 - hereafter C09, for recent reviews and references). One of the main aims of these studies was to collect as much as possible information on the GCs in M31 and compare it with our knowledge of the GCs in the Galaxy, so as to derive better insight into the formation and (chemical and dynamical) evolution of these two spiral galaxies and possibly of galaxies in general. The advent of the Hubble Space Telescope provided the unprecedented opportunity to obtain colour-magnitude diagrams (CMD) of M31 clusters, thus adding a completely new perspective to this research.

Substantial contributions in this field have been made by many investigators. At present, sufficiently accurate visual CMDs for a meaningful comparison with their Galactic counterparts have been published for 35 GCs in M31. Except for

Send offprint requests to: S. Perina

<sup>\*</sup> Based on observations made with the NASA/ESA *Hubble Space Telescope*, obtained from the data archive at the Space Telescope Science Institute. STScI is operated by the Association of Universities for Research in Astronomy, Inc., under NASA contract NAS 5-26555.”

<sup>\*\*</sup> RBC Version 3.5 available at: [www.bo.astro.it/M31](http://www.bo.astro.it/M31)

one that was observed from the ground (MGC1, Martin et al. 2006), a good fraction of these have been obtained with the HST-WFPC2 (Ajhar et al. 1996, Rich et al. 1996, Fusi Pecci et al. 1996, Holland et al. 1997, Jablonka et al. 2000, Meylan et al. 2001, Rich et al. 2005) until the better resolution and sensitivity of the ACS allowed even more accurate CMDs at fainter limiting magnitudes (Brown et al. 2004; Huxor et al. 2004, 2005, 2008; Galletti et al. 2006b; Mackey et al. 2006, 2007).

In addition to photometric quality, which is essential for the analysis of individual objects, a good statistical coverage is also important for a better understanding of the GC system. To increase the sample of M31 GCs with a CMD of individual member stars, we searched the HST archive for ACS images of objects that are listed in the Revised Bologna Catalogue of M31 clusters (RBC, see G04). We found useful ACS images containing 69 such objects (see Fig. 1). The retrieved material allowed us to confirm or revise the classification of all of them and to obtain CMD of individual stars for 17, 11 likely old globulars, and 6 young luminous clusters (like those discussed in Williams & Hodge 2001; Fusi Pecci et al 2005 and Perina et al. 2009a). This paper is devoted to the analysis of these data.

In Sect. 2 we present the target list, and in Sect. 3 we describe the adopted reduction procedures that yielded the CMDs. Section 4 is devoted to describe the method we have used to estimate the metallicity, reddening, and distance from each in-

dividual CMD for which a sufficiently reliable decontamination from the non-member field components was feasible. In Sect. 5 specific notes and comments on the results are presented for each of the 11 GCs (the primary targets) and for the other objects for which a sufficiently meaningful photometry was carried out. In Sect. 6 we discuss a possible connection between a few clusters and a large substructure recently found in M31. Finally, Sect. 7 contains some general considerations and conclusions.

## 2. The targets

A search by coordinates allowed us to find ACS images<sup>1</sup> for 69 entries of the RBC V3.5, independently of their original classification (see G04, and Galleti et al. 2006a). In two cases the images revealed that there were two catalogue entries referring to the same object (i.e. B521=SK034A, and B522=SK038A), thus reducing the number of real objects to 67. Four confirmed clusters classified as candidate "intermediate-age GCs" by Puzia et al. (2005), and for which we have obtained good CMDs, have been excluded from the list as they will be the subject of a dedicated study (Perina et al. 2009b, in preparation).

Eighteen of the remaining 63 objects, namely B004D, B253, B034D, SK102C, G137, SK107C, B102, SK094B, B072D, SK077D, SK078D, SK079D, SK120B, SK083D, B175, SK079A, M047, and SK181B, are not *bona fide* clusters: their original RBC classification has been confirmed or revised based on the high resolution ACS images. The results of this analysis are summarised in Table 2 where we report their old and new classification flag.

Twenty of the remaining 45 objects are unequivocally confirmed as *bona fide* clusters (B037, B041, B042, B056D, B061, B063, B082, B094, SK048A, B130, B185, B198, B203, B206, B213, B215, B231, B234, B522=SK038A, and SK036A, see Fig. 3) and we obtained photometry of individual stars from the respective images, however we were unable to find an annulus around the cluster centre where the population of the cluster could be disentangled from the population of the surrounding field. In general this is due to the extreme compactness of the clusters, preventing to obtain good photometry for a sufficient number of stars even in the outermost coroneae, but also the density of the background population plays a role. For five additional clusters, e.g. B147, B151, B162, B169, B171 (Fig. 3), located in the bulge of M31, at projected distances  $R=7.8', 7.29', 7.17', 6.31'$  and  $9.95'$  from the centre, the overall crowding was so high that it resulted impossible to carry out any meaningful photometry even in the field, with the method adopted here.

The remaining 20 objects are the main subject of the present analysis and are subdivided as follows:

- Eleven *bona fide* clusters for which we could obtain a meaningful CMD, albeit of varying accuracy<sup>2</sup>, and that were revealed by their CMD to be likely classical old globulars (i.e. having ages of several Gyr). These are the "primary targets" discussed in this paper, namely B008, B010, B023, B088, B158, B220, B224, B225, B255D, B366, and B407, according to the RBC nomenclature.
- Nine *bona fide* clusters that were listed as candidate young clusters (age  $\leq 2$  Gyr) by some previous study (Fig. 4). Five of them, namely B049, B057, B090, B367, B458 were included in the list of the so-called "Blue Luminous Compact

Clusters" (Fusi Pecci et al. 2005); three of them, namely B521=SK034A, M039=KHM31-516 (Krienke and Hodge 2008), and M050 were classified as "young" by C09 (see Table 6); and one, B515=KHM31-409, was included in the list of possible young/open clusters of Krienke and Hodge (2008). For six of them (B039, B049, M050, B367, B458, and B521) we were able to derive a CMD in which the cluster population can be identified and we can confirm their young age, while for the other three we obtained useful photometry only for the surrounding field.

Going back to the 11 "primary target" GCs discussed in detail in the present study, most of them lie close to the galactic plane of M31, as shown in Fig. 1. Three of them have been observed with the ACS/HRC and eight with the ACS/WFC. Their V images are shown in Fig. 2 and their HST data are listed in Table 1, together with their integrated magnitudes and colours taken from the RBC, when available. Similar data for all the other 52 targets considered in this paper are reported in Table 2.

## 3. Data reduction and the colour-magnitude diagrams

Data reduction has been performed on the prereduced images provided by STScI, using the ACS module of DOLPHOT<sup>3</sup> (Dolphin 2000a), a point-spread function fitting package specifically devoted to the photometry of HST data. The package identifies the sources above a fixed flux threshold on a stacked image and performs the photometry on individual frames, accounts for the hot-pixel and cosmic-ray masking information attached to the observational material, automatically applies the correction for the Charge Transfer Efficiency (CTE, Dolphin 2000b) and transforms instrumental magnitude to the VEGAMAG and standard BVI system using the transformations by Sirianni et al. (2005). In the following we use BVI photometry.

We fixed the threshold for the search of sources on the images at  $3\sigma$  above the background. DOLPHOT provides as output the magnitudes and positions of the detected sources, as well as a number of quality parameters for a suitable sample selection, in view of the actual scientific objective one has in mind. Here we selected all the sources having valid magnitude measurements in both passbands, global quality flag = 1 (i.e., best measured stars), *crowding* parameter  $\leq 0.3$ ,  $\chi^2 < 1.5$  if  $V < 22.5$ ,  $\chi^2 < 2.5$  for brighter stars, and *sharpness* parameter between -0.3 and 0.3 (see Dolphin 2000b for details on the parameters). This selection cleans the sample from the vast majority of spurious and/or bad measured sources without significant loss of information, and it has been found to be appropriate for the whole data set.

The limiting magnitudes of our photometry range from  $V \sim 26$  for the fields observed with relatively short exposure times, to  $V \sim 27.5$  for the deepest ones. The internal photometric errors of individual measures are in general within the range 0.01 - 0.08 mag for stars brighter than  $V=26$ , (see Fig. 5) depending quite strongly on the degree of crowding. However, errors increase rapidly for fainter stars, along with the impact of blending. Since we are mainly interested in the position and morphology of the main CMD branches we have not performed artificial stars experiments to study in detail the completeness of the samples as a function of magnitude. However, based on simple tests and on our previous experience, we are confident that in all

<sup>1</sup> released until June 2007 from the HST Archive.

<sup>2</sup> depending on the cluster characteristics, the crowding conditions and the surface density of the surrounding field.

<sup>3</sup> See <http://purcell.as.arizona.edu/dolphot/>.

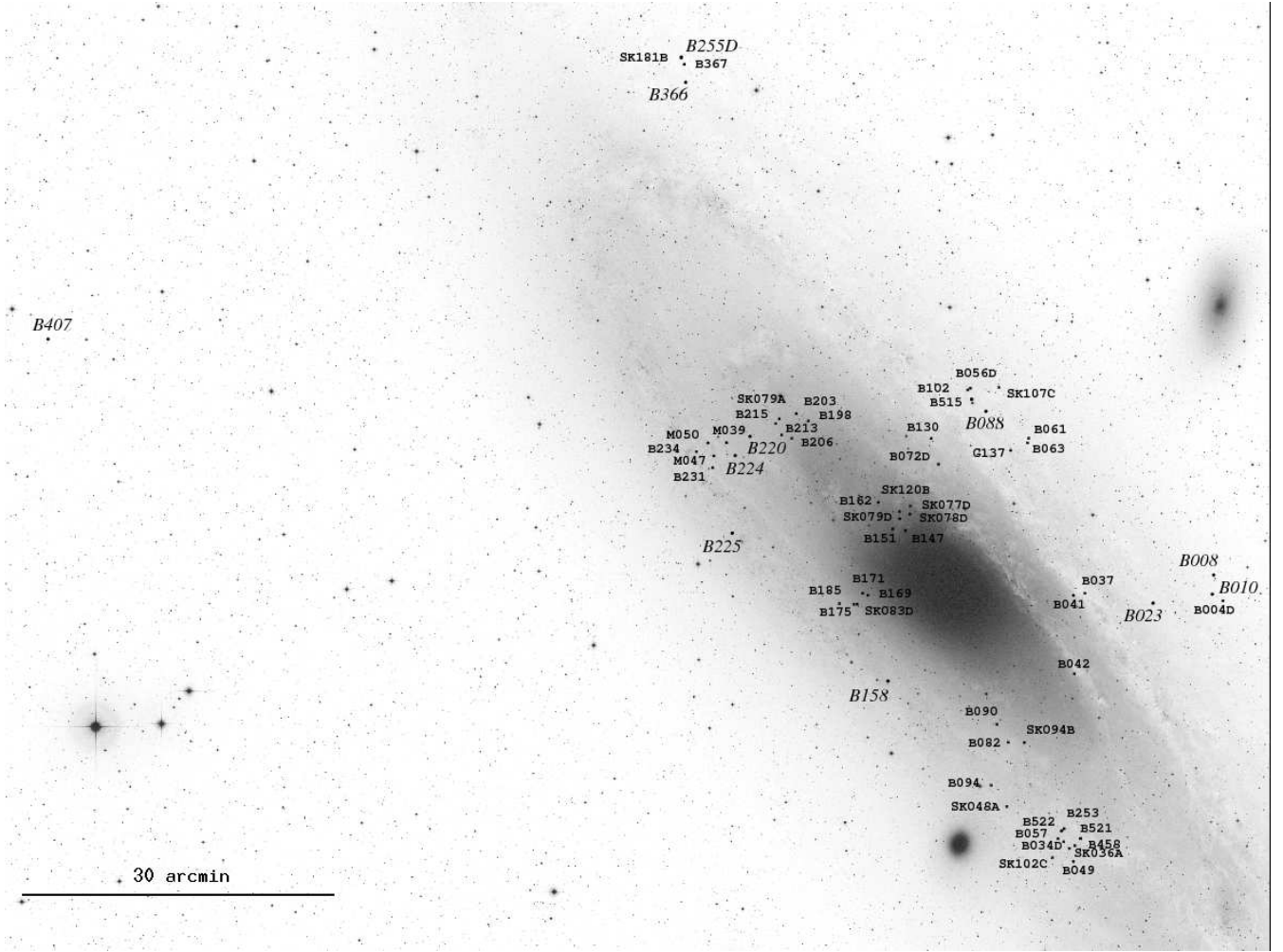


**Fig. 1.** The location of the 11 primary target globular clusters, marked in italics + 52 secondary targets (see Sect.2 and 5), projected against the body of M31, with North up and East to the left.

**Table 1.** The primary target M31 GCs. ID, coordinates and photometry are from G04; [Fe/H] are from (<sup>a</sup>): Perrett et al. (2002), and (<sup>b</sup>): Huchra, Brodie & Kent(1991).

ID	RA (J2000)	Dec (J2000)	X arcmin	Y arcmin	V	(B-V)	(V-I)	[Fe/H]	ACS camera, bands(total $t_{exp}$ )	PID
B008-G60	00 40 30.54	+41 16 09.7	-15.41	19.86	16.56	1.10	1.05	-0.41 <sup>a</sup>	WFC,F606W(3250s),F435W(7260s)	10407
B010-G62	00 40 31.56	+41 14 22.3	-16.71	18.62	16.66	0.84	1.18	-1.87 <sup>b</sup>	WFC,F606W(3250s),F435W(7260s)	10407
B023-G78	00 41 01.26	+41 13 45.3	-13.78	13.82	14.22	1.18	1.65	-0.92 <sup>b</sup>	HRC,F606W(2020s),F814W(2860s)	9719
B088-G150	00 42 21.10	+41 32 14.3	10.00	13.32	15.42	1.12	1.47	-2.17 <sup>b</sup>	WFC,F606W(2370s),F814W(2370s)	10260
B158-G213	00 43 14.47	+41 07 20.6	-3.45	-9.90	14.70	0.86	1.15	-1.08 <sup>b</sup>	HRC,F606W(2020s),F814W(2860s)	9719
B220-G275	00 44 19.49	+41 30 35.7	22.38	-5.13	16.55	0.78	1.06	-2.07 <sup>b</sup>	WFC,F606W(1860s),F435W(2910s)	10407
B224-G279	00 44 27.21	+41 28 50.6	21.90	-7.35	15.45	0.79	1.03	-1.90 <sup>b</sup>	WFC,F606W(1860s),F435W(2910s)	10407
B225-G280	00 44 29.78	+41 21 36.6	16.52	-12.21	14.15	1.01	1.39	-0.70 <sup>b</sup>	HRC,F606W(2020s),F814W(2860s)	9719
B255D-D072	00 44 48.55	+42 06 13.3	53.70	12.71	17.92				WFC,F606W(1850s),F435W(2920s)	10407
B366-G291	00 44 46.72	+42 03 50.3	51.62	11.49	15.99	0.81	1.01	-1.39 <sup>b</sup>	WFC,F606W(1850s),F435W(2920s)	10407
B407-G352	00 50 09.98	+41 41 01.1	71.54	-49.72	16.05	0.90	1.22	-0.85 <sup>b</sup>	WFC,F606W(2400s),F814W(5100s)	9458

of the considered cases the completeness is more than sufficient ( $\geq 70\%$ ) to achieve our scientific goals for  $V \leq 26$ .

To have an idea of the characteristic sizes of the clusters we estimated half-light radii –  $R_h$  (see Table 4) by aperture photometry over concentric annuli centered on the cluster and extended out to sufficiently large distances to properly sample the

background. This approach is quite rough, nevertheless the values obtained here for the 5 clusters (B023, B088, B158, B225, B407) in common with Barmby et al. (2007) agree within 0.05 arcseconds (i.e. to better than 0.2 pc at the M31 distance) in all cases.

**Table 2.** The additional targets (see Sect. 2) grouped according to their location within the same-exposure field. All of them were observed with WFC@ACS on HST. ID, coordinates and photometry are from Galleti et al. (2004). We note the double identifications B521=SK034A and B522=SK038A.

ID	RA (J2000)	Dec (J2000)	X arcmin	Y arcmin	V	(B-V)	(V-I)	[Fe/H]	type <sup>a</sup>	bands(exptime)	PID	Datasets
B004D-V223	00 40 26.41	+41 13 42.7	-17.82	18.98	18.81	1.18			4	F606W(3250s),F435W(7260s)	10407	J96Q07010,J96Q07020
B037-V327	00 41 35.00	+41 14 54.9	-8.98	9.51	16.82	2.05	2.63	-1.07 <sup>a</sup>	1	F606W(2370s),F814W(2370s)	10260	J8Z003010,J8Z003020
B041-G103	00 41 40.73	+41 14 45.8	-8.44	8.57	17.65	0.97	1.18	-1.22 <sup>a</sup>	1	F606W(2370s),F814W(2370s)	10260	J8Z019010,J8Z019010
B042-G104	00 41 41.69	+41 07 25.8	-14.12	3.93	16.29	1.48	1.89	-1.09 <sup>b</sup>	1	F606W(2370s),F814W(2370s)	10260	J8Z060010,J8Z022010
B057-G118 <sup>†</sup>	00 41 52.84	+40 52 04.6	-24.96	-7.15	17.64	0.69	0.99	-2.12 <sup>a</sup>	1	F606W(2110s),F435W(2672s)	10407	J96Q06010,J96Q06020
B253	00 41 49.63	+40 52 59.7	-24.60	-6.11	18.01		0.55		6	F606W(2110s),F435W(2672s)	10407	J96Q06010,J96Q06020
B034D	00 41 50.13	+40 51 46.7	-25.51	-6.93	17.50				6	F606W(2110s),F435W(2672s)	10407	J96Q06010,J96Q06020
B522-SK038A	00 41 50.94	+40 52 48.3	-24.60	-6.42	17.85				1(2)	F606W(2110s),F435W(2672s)	10407	J96Q06010,J96Q06020
SK102C	00 41 55.92	+40 50 19.7	-25.98	-8.68	15.22	0.76	0.85		6(2)	F606W(2110s),F435W(2672s)	10407	J96Q06010,J96Q06020
B521-SK034A	00 41 41.67	+40 52 01.4	-26.29	-5.51					1(2) <sup>‡</sup>	F606W(2110s),F435W(2672s)	10407	J96Q06010,J96Q06020
B458-D049 <sup>†</sup>	00 41 44.61	+40 51 22.3	-26.47	-6.35	17.84	0.49	0.57	-1.18 <sup>a</sup>	1	F606W(2110s),F435W(2672s)	10407	J96Q06010,J96Q06020
B049-G112 <sup>†</sup>	00 41 45.60	+40 49 53.7	-27.52	-7.41	17.56	0.52	0.69	-2.14 <sup>a</sup>	1	F606W(2110s),F435W(2672s)	10407	J96Q06010,J96Q06020
SK036A	00 41 47.34	+40 51 07.5	-26.35	-6.91	19.43	1.01	1.13		1	F606W(2110s),F435W(2672s)	10407	J96Q06010,J96Q06020
B063-G124	00 42 00.80	+41 29 09.5	5.24	14.43	15.66	1.21	1.58	-0.87 <sup>b</sup>	1	F606W(2370s),F814W(2370s)	10260	J8Z008010,J8Z024010
B061-G122	00 42 00.20	+41 29 35.5	5.51	14.79	16.61	1.12	1.49	-0.79 <sup>b</sup>	1	F606W(2370s),F814W(2370s)	10260	J8Z008010,J8Z024010
G137	00 42 09.43	+41 28 30.4	5.71	12.76	17.81	-0.02			5	F606W(2370s),F814W(2370s)	10260	J8Z008010,J8Z024010
SK107C	00 42 14.18	+41 34 26.3	10.94	15.70	19.65	0.80	0.89		6(2)	F606W(2370s),F814W(2370s)	10260	J8Z007010,J8Z023010
B515 <sup>1</sup>	00 42 28.05	+41 33 24.5	11.72	13.02	18.67 <sup>2</sup>				1	F606W(2370s),F814W(2370s)	10260	J8Z007010,J8Z023010
B056D	00 42 28.45	+41 34 27.2	12.59	13.60	18.70				1	F606W(2370s),F814W(2370s)	10260	J8Z007010,J8Z023010
B102	00 42 29.85	+41 34 18.2	12.64	13.30	16.58	0.62	0.95		7	F606W(2370s),F814W(2370s)	10260	J8Z007010,J8Z023010
B082-G144	00 42 15.79	+41 01 14.3	-15.06	-4.94	15.54	1.56	1.91	-0.86 <sup>b</sup>	1	F606W(2370s),F814W(2370s)	10260	J8Z004010,J8Z020010
SK094B	00 42 07.81	+41 01 10.0	-16.05	-3.80	18.13	1.11	1.24	-0.86 <sup>b</sup>	4(2)	F606W(2370s),F814W(2370s)	10260	J8Z004010,J8Z020010
B090 <sup>†</sup>	00 42 21.12	+41 02 57.3	-13.09	-4.68	18.80		1.64	-1.39 <sup>a</sup>	1	F606W(2370s),F814W(2370s)	10260	J8Z004010,J8Z020010
B094-G156	00 42 25.01	+40 57 17.2	-17.11	-8.74	15.55	0.97	1.26	-0.41 <sup>b</sup>	1	F555W( 413s),F814W(502s)	10273	J92GB9BRQ,J92GB9BPQ
SK048A	00 42 17.59	+40 55 15.3	-19.58	-8.89	18.49	0.65	0.74		1	F555W( 413s),F814W(502s)	10273	J92GB9BRQ,J92GB9BPQ
B130-G188	00 42 48.91	+41 29 52.9	11.35	7.77	16.93	1.15	1.41	-1.28 <sup>a</sup>	1	F555W( 413s),F814W(502s)	10273	J92GB6ZLQ,J92GB6ZLNQ
B072D	00 42 45.78	+41 27 26.9	9.07	6.74	18.50			-1.28 <sup>a</sup>	3(4) <sup>3</sup>	F555W( 413s),F814W(502s)	10273	J92GB6ZLQ,J92GB6ZLNQ
B151-G205	00 43 09.64	+41 21 32.6	7.17	-0.43	14.83	1.23	1.45	-0.75 <sup>b</sup>	1	F606W(2370s),F814W(2370s)	10260	J8Z005010,J8Z021010
B147-G199	00 43 03.31	+41 21 21.5	6.30	0.39	15.80	0.84	1.27	-0.24 <sup>b</sup>	1	F606W(2370s),F814W(2370s)	10260	J8Z005010,J8Z021010
SK077D	00 43 00.52	+41 23 37.6	7.76	2.20	17.66	0.41	0.48		6	F606W(2370s),F814W(2370s)	10260	J8Z005010,J8Z021010
SK078D	00 43 00.86	+41 22 52.3	7.20	1.69	18.13	0.69	0.78		6	F606W(2370s),F814W(2370s)	10260	J8Z005010,J8Z021010
SK079D	00 43 06.04	+41 22 28.7	7.49	0.68	18.67	1.43	1.62		6	F606W(2370s),F814W(2370s)	10260	J8Z005010,J8Z021010
SK120B	00 43 05.97	+41 23 08.1	8.00	1.10	19.33	0.82	0.92		6(2)	F606W(2370s),F814W(2370s)	10260	J8Z005010,J8Z021010
B162-G216	00 43 16.42	+41 24 04.2	9.95	0.13	17.48	1.05	1.34		1	F606W(2370s),F814W(2370s)	10260	J8Z005010,J8Z021010
B171-G222	00 43 25.67	+41 15 37.4	4.37	-6.45	15.28	0.99	1.58	-0.48 <sup>b</sup>	1	F606W(3396s),F435W(4476s)	10407	J96Q03010,J96Q03020
B169	00 43 23.06	+41 15 25.5	3.91	-6.19	17.08	1.23	1.31		1	F606W(3396s),F435W(4476s)	10407	J96Q03010,J96Q03020
SK083D	00 43 28.60	+41 14 36.7	3.92	-7.51	14.64	1.05	1.17		6	F606W(3396s),F435W(4476s)	10407	J96Q03010,J96Q03020
B175	00 43 30.18	+41 14 36.4	4.09	-7.74	16.80	0.80			6	F606W(3396s),F435W(4476s)	10407	J96Q03010,J96Q03020
B185-G235	00 43 37.41	+41 14 43.3	5.02	-8.74	15.54	0.94	1.18	-1.03 <sup>b</sup>	1	F606W(3396s),F435W(4476s)	10407	J96Q03010,J96Q03020
B206-G257	00 43 58.70	+41 30 18.0	19.74	-2.25	15.06	0.80	1.03	-1.45 <sup>b</sup>	1	F606W(2110s),F435W(2672s)	10407	J96Q05010,J96Q05020
B198-G249	00 43 50.07	+41 31 53.1	19.99	-0.00	17.55	0.60	1.11	-1.13 <sup>a</sup>	1	F606W(2110s),F435W(2672s)	10407	J96Q05010,J96Q05020
B203-G252	00 43 56.00	+41 32 36.0	21.23	-0.43	16.68	0.93	1.20	-0.90 <sup>a</sup>	1	F606W(2110s),F435W(2672s)	10407	J96Q05010,J96Q05020
B213-G264	00 44 03.62	+41 30 38.9	20.58	-2.76	16.78	1.05	1.29	-0.99 <sup>b</sup>	1	F606W(2110s),F435W(2672s)	10407	J96Q05010,J96Q05020
SK079A	00 44 04.58	+41 32 09.3	21.88	-1.97	18.63	1.11	1.23		6(1)	F606W(2110s),F435W(2672s)	10407	J96Q05010,J96Q05020
B215-G266	00 44 06.44	+41 31 43.9	21.76	-2.51	17.13	1.02	1.20		1	F606W(2110s),F435W(2672s)	10407	J96Q05010,J96Q05020
M039 <sup>4</sup>	00 44 31.30	+41 30 04.6	23.34	-7.18	18.94	1.11	-0.53		1(2) <sup>‡</sup>	F606W(1860s),F435W(2910s)	10407	J96Q02010,J96Q02020
B234-G290	00 44 46.50	+41 29 18.3	24.50	-9.90	16.78	1.00	1.18	-0.95 <sup>a</sup>	1	F606W(3315s),F435W(4560s)	10407	J96Q04010,J96Q04020
M047	00 44 37.85	+41 28 52.1	23.16	-8.90	18.84		1.2		2 <sup>5</sup>	F435W(4560s),F606W(3315s)	10407	J96Q04010,J96Q04020
B231-G285	00 44 38.61	+41 27 46.8	22.39	-9.68	17.27	0.84	1.14	-1.49 <sup>a</sup>	1	F435W(4560s),F606W(3315s)	10407	J96Q04010,J96Q04020
M050	00 44 40.59	+41 30 06.0	24.44	-8.53	18.71		0.40		1(2) <sup>‡</sup>	F606W(3315s),F435W(4560s)	10407	J96Q04010,J96Q04020
B367-G292 <sup>†</sup>	00 44 47.18	+42 05 31.9	53.00	12.48	18.45	0.32	1.30	-2.32 <sup>a</sup>	1	F606W(1850s),F435W(2920s)	10407	J96Q01010,J96Q01020
SK181B	00 44 48.64	+42 06 08.1	53.64	12.64	19.18	1.28	1.46		6(2)	F606W(1850s),F435W(2920s)	10407	J96Q01010,J96Q01020

(<sup>a</sup>): Perrett et al. (2002); (<sup>b</sup>): Huchra, Brodie & Kent(1991); <sup>†</sup>: BLCC, Fusi Pecci et al. (2005)

(<sup>\*</sup>): classification, coded as follows: 1- confirmed cluster; 2- gc candidate; 3- controversial object 4- galaxy; 5- HII region; 6- star; 7- asterism; <sup>‡</sup>: young cluster (from this paper and/or Caldwell et al.(2009)). In parentheses is enclosed the previous RBCv3.5 value.

(<sup>1</sup>): identified as KHM31-409 in Krienke&Hodge (2008), tab.4; (<sup>2</sup>): V mag from Krienke&Hodge (2008), tab.4; (<sup>3</sup>): B072D, that was originally classified as a galaxy by Huxor et al. (2008), looks like a cluster, as noted also by Caldwell et al. (2009). Radial velocity is necessary in our view to yield its firm confirmation; (<sup>4</sup>): identified as KHM31-516 in Krienke & Hodge (2008), tab.4; (<sup>5</sup>): classified as globular cluster by Caldwell et al. (2009).

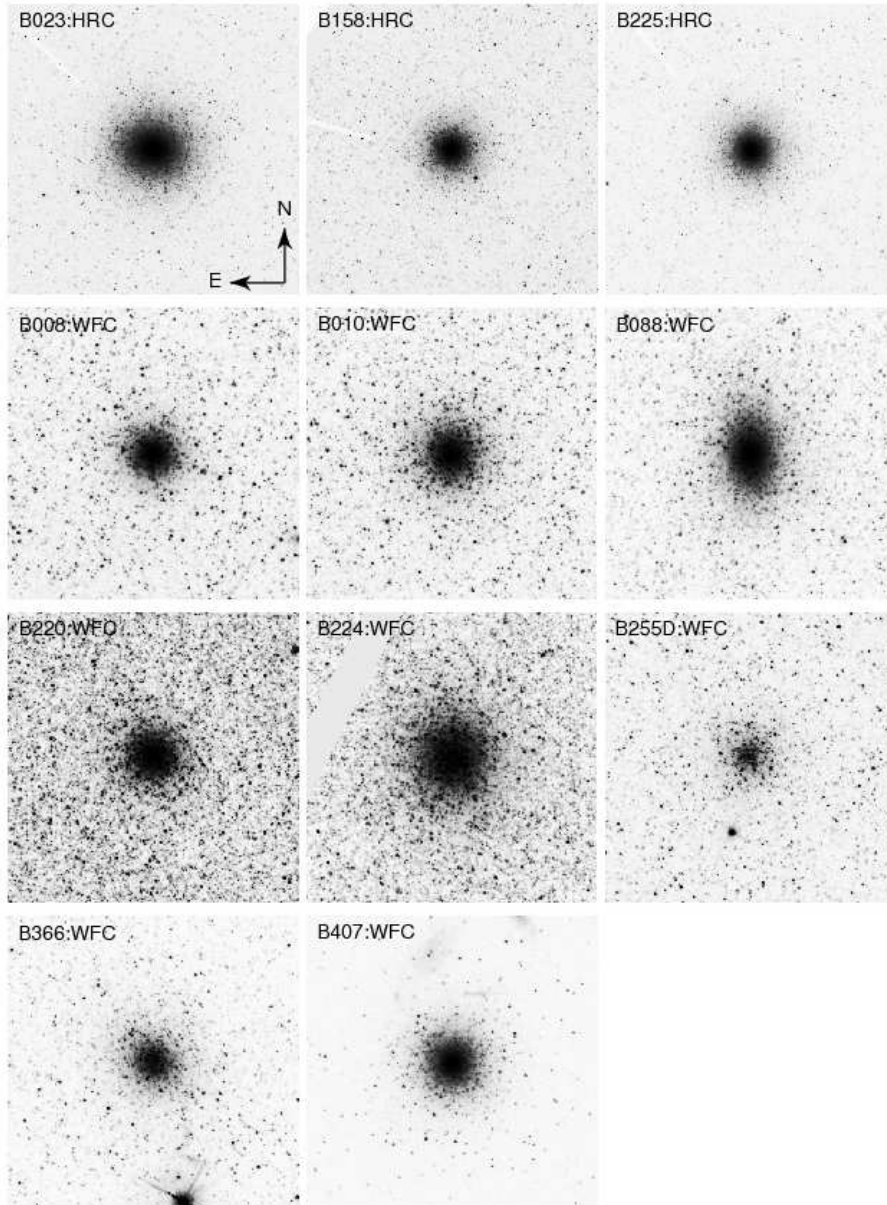


**Fig. 2.** V band (F606W) images of the 11 M31 GCs analysed in the present study (the primary targets). The cluster and ACS camera identification are shown in each subraster. Each image covers  $20'' \times 20''$  ( $20'' = 76$  pc at the assumed M31 distance modulus of 24.47). North is up and East to the left.

The individual CMDs are shown in Figs. 6 and 7, where the cluster and field stellar populations are indicated with different symbols (filled black and open grey circles, respectively). The cluster CMDs shown in these figures sample the stellar population within an annulus around the cluster centre where the cluster members are more readily distinguishable with respect to the surrounding field. The inner limit of the annulus is set by the crowding level that prevents from performing useful photometry in the most central region of the cluster, the outer limit is set by the limiting radius of the cluster and by the need to avoid contamination by the surrounding field population. The inner and outer radii of the adopted annuli are indicated for each cluster. The field population is measured on an outer concentric annulus having the same area as the cluster annulus. In all the CMDs shown in Figs. 6 and 7 the cluster population can be distinguished from the field. In most cases the clusters show a

thinner and much steeper RGB with respect to the field, and in many cases a Blue HB is visible, that has no (or much weaker) counterpart in the field population.

Before proceeding with the analysis of the cluster properties (discussed in Sect. 3), we have applied the field decontamination procedure described in Bellazzini et al. (1999). This method is based on a clipping routine which, making use of the local density on the CMDs of the field and of the cluster, computes the probability that a given star is a member of the cluster and retains or rejects stars from the cluster CMD according to that. To verify the reliability of this procedure we carried out several decontamination tests using different areas of the field and different techniques. In particular we applied to the most contaminated clusters a statistical subtraction procedure based on a Monte Carlo approach, where up to 5000 field-subtraction trials were used, thus obtaining globular cluster measured samples

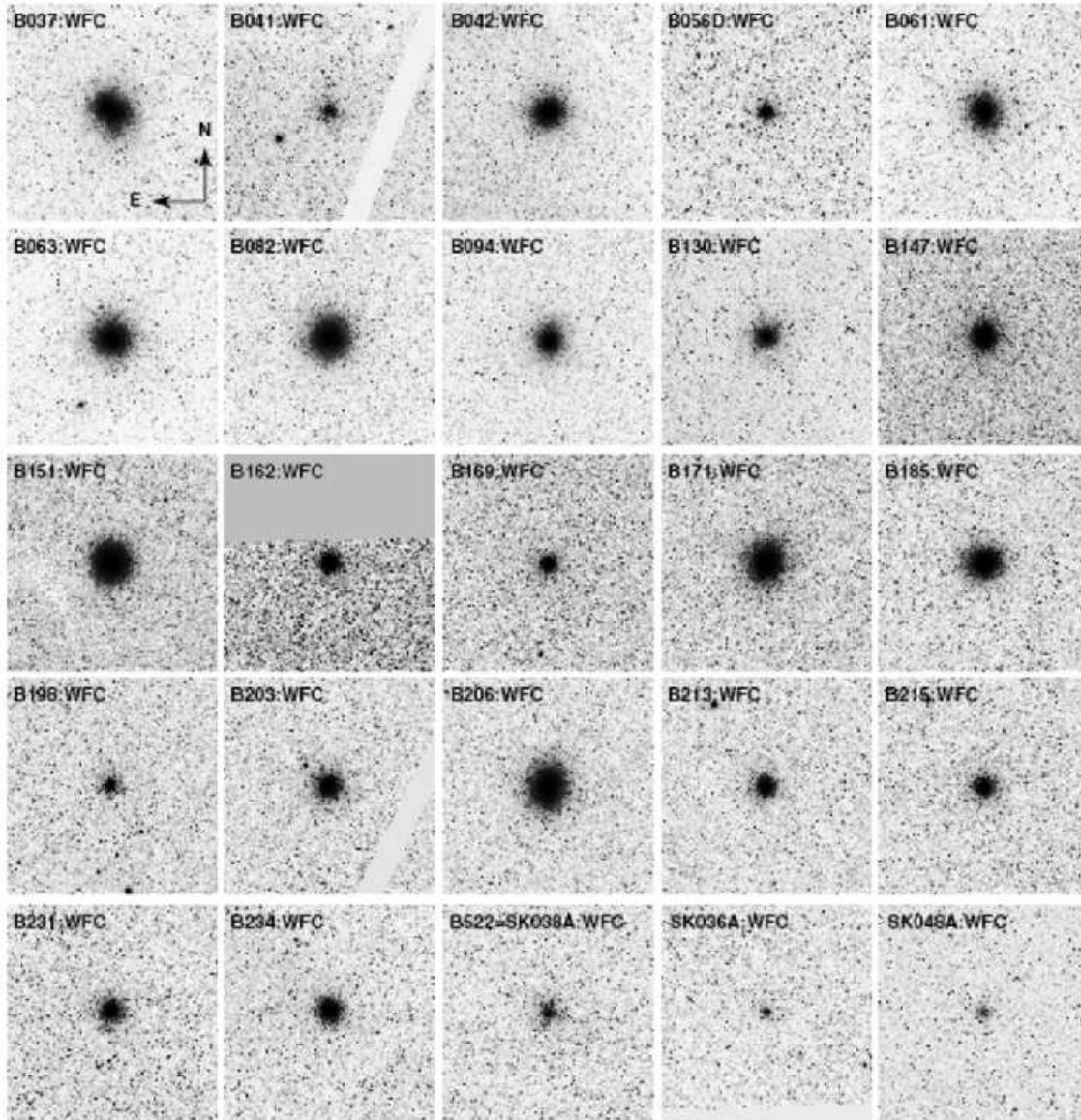


**Fig. 3.** Same as in Fig. 2 for 25 additional M31 globular clusters (see Sect. 2 ).

weighted by a statistical membership likelihood. Figs. 9 and 10 show that the decontamination of our primary targets was quite successful, providing “clean” CMDs in which the main cluster branches are more clearly identified (the individual cases are briefly discussed in Sect. 5). Therefore, the following analysis is based on the decontaminated CMDs.

### 3.1. Comparison with Fuentes-Carrera et al. (2008) photometry

While carrying out the present analysis, independent photometry of three objects included in our primary sample (B023=G078, B158=G213, B225=G280) was produced by Fuentes-Carrera et al. (2008) based on the same data set. Both CMDs for each of these three clusters are shown side by side in Fig. 8, showing an excellent degree of consistency in magnitude and colour extension and in the quality of individual star photometry. The close coincidence of the main branches and even of most of the detected stars testifies the strict similarity and agreement of these two independent photometries.

Fuentes-Carrera et al. have focussed their analysis on the claimed existence of metallicity spreads in these very bright and populous GCs, based on the intrinsic width of the main branches. Although the quality of their data reduction is comparable to ours, we have not dealt with this aspect which is beyond the scope of the present study. We refer the interested reader to their work for a detailed discussion of this topic.

## 4. M31 vs. Galactic GCs: direct comparisons of the CMDs

We estimate the distance, metallicity, and reddening of our primary clusters by comparison with a set of CMD templates of well studied Galactic GCs, similarly to Rich et al. (2005), and Mackey et al. (2006, 2007). Relying on the hypothesis that the considered clusters are of similar nature as their Galactic counterparts we searched for the set of parameters ( $(m - M)_0$ ,  $E(B - V)$  and  $[\text{Fe}/\text{H}]$ ) producing the best match between the observed RGBs and HBs and the ridge lines of the template clusters in the absolute plane, given the direction of the red-



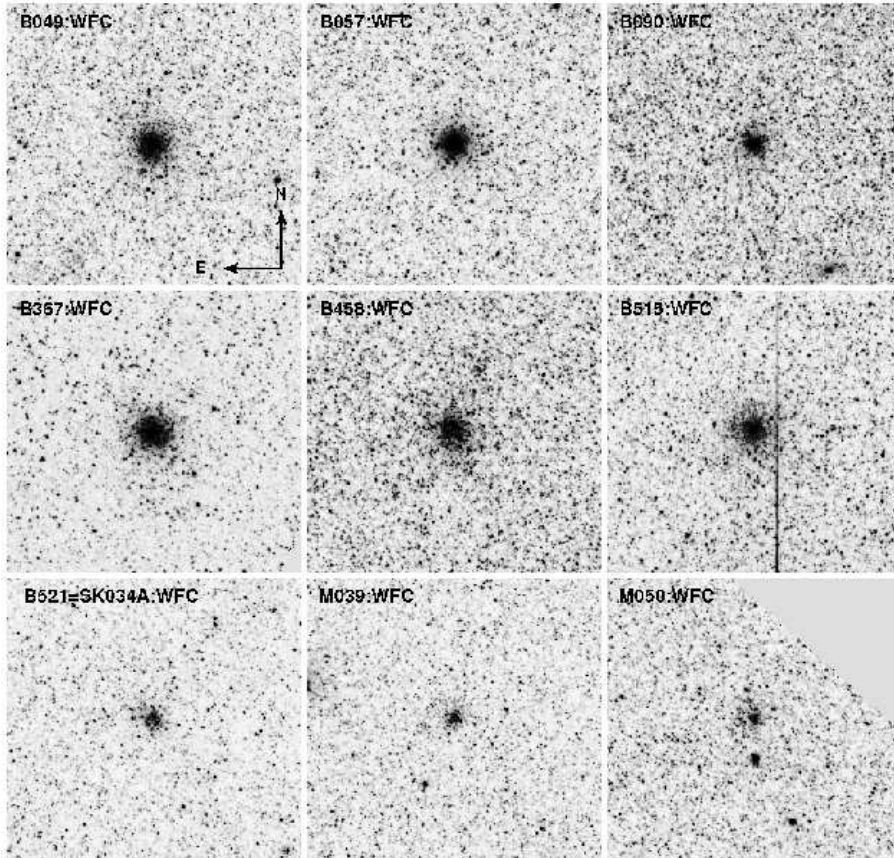


**Fig. 4.** V band (F606W) images of the 9 candidate young clusters (see Sect. 5.12). The cluster and ACS camera identification are shown in each subraster. Each image covers  $20'' \times 20''$ .

dening vector  $A_V = 3.1E(B - V)$ ,  $A_I = 1.94E(B - V)$  and  $E(V - I) = 1.375E(B - V)$  (Schlegel et al. 1998).

The best match was judged by eye guided by (extensive) experience, as this approach is much more robust than most automated algorithms in presence of significant residuals from the decontamination procedure. The steepness of the RGB is of great help in judging if the branch is red because of high metallicity or because of high reddening; the fact that the HB match is mostly sensitive to vertical (magnitude) shifts, while the RGB is mostly sensitive to horizontal (colour) shifts also provides a useful guide to the solution. Colour and magnitude shifts are applied iteratively until a satisfactory match with any RGB and HB template is found: from these shifts we obtain estimates of the reddening and distance, while the metallicity is estimated by interpolation between the two RGB ridge lines bracketing the observed RGB locus.

As starting values for the iterative procedure we have used  $E(B - V) = 0.08$  for the foreground reddening (Barmby et al. 2007; Burstein and Heiles 1984), and the distance modulus  $\mu_0 = 24.47$  mag for all the M31 clusters (McConnachie et al. 2005). The ridge lines of the reference GGCs were assembled from the observed CMDs (Piotto et al. 2002 for BV photometric data, and Rosenberg et al. 2000a,b for VI) that were shifted to the absolute reference frame by correcting for reddening and distance using the values listed in Table 3. These reference GGCs have been chosen to provide a sufficiently fine and regular sampling over a wide enough range of metallicities for a correct characterization of the target GGCs.

**Table 3.** Reference grid of template Galactic globular clusters.

ID	[Fe/H] dex	$E(B - V)$ mag	$\mu_V$ mag	Phot.
NGC7078 (M15)	-2.16	0.10	15.37	BV
NGC6397	-1.91	0.18	12.36	VI
NGC5824	-1.87	0.13	17.93	BV
NGC5272 (M3)	-1.66	0.01	15.12	VI
NGC6205 (M13)	-1.65	0.02	14.48	BV
NGC5904 (M5)	-1.40	0.03	14.46	VI,BV
NGC6723	-1.12	0.05	14.85	BV
47 Tuc	-0.71	0.04	13.37	VI,BV
NGC6624	-0.35	0.28	15.36	BV
NGC6553	-0.29	0.63	15.83	VI

NOTES: Metallicities are from Zinn (1985); all other parameters are from Harris (1996) (online update 2003). VI photometry is from Rosenberg et al.(2000a,b); B,V photometry is from Piotto et al. (2002).

In Figs. 9 and 10 we show the field decontaminated CMDs and, overplotted, the reference grid of GGC ridge lines, where the bracketing RGB reference clusters are highlighted. The values of metallicity, reddening and distance corresponding to the best match are also reported in each individual panel, as well as in Table 4; the typical uncertainty on the distance modulus is  $\pm 0.2$  mag,  $\pm 0.04$  mag in  $E(B - V)$ , and  $\pm 0.25$  dex in metallicity. We think that the solutions presented in Fig. 9 and Fig. 10 are

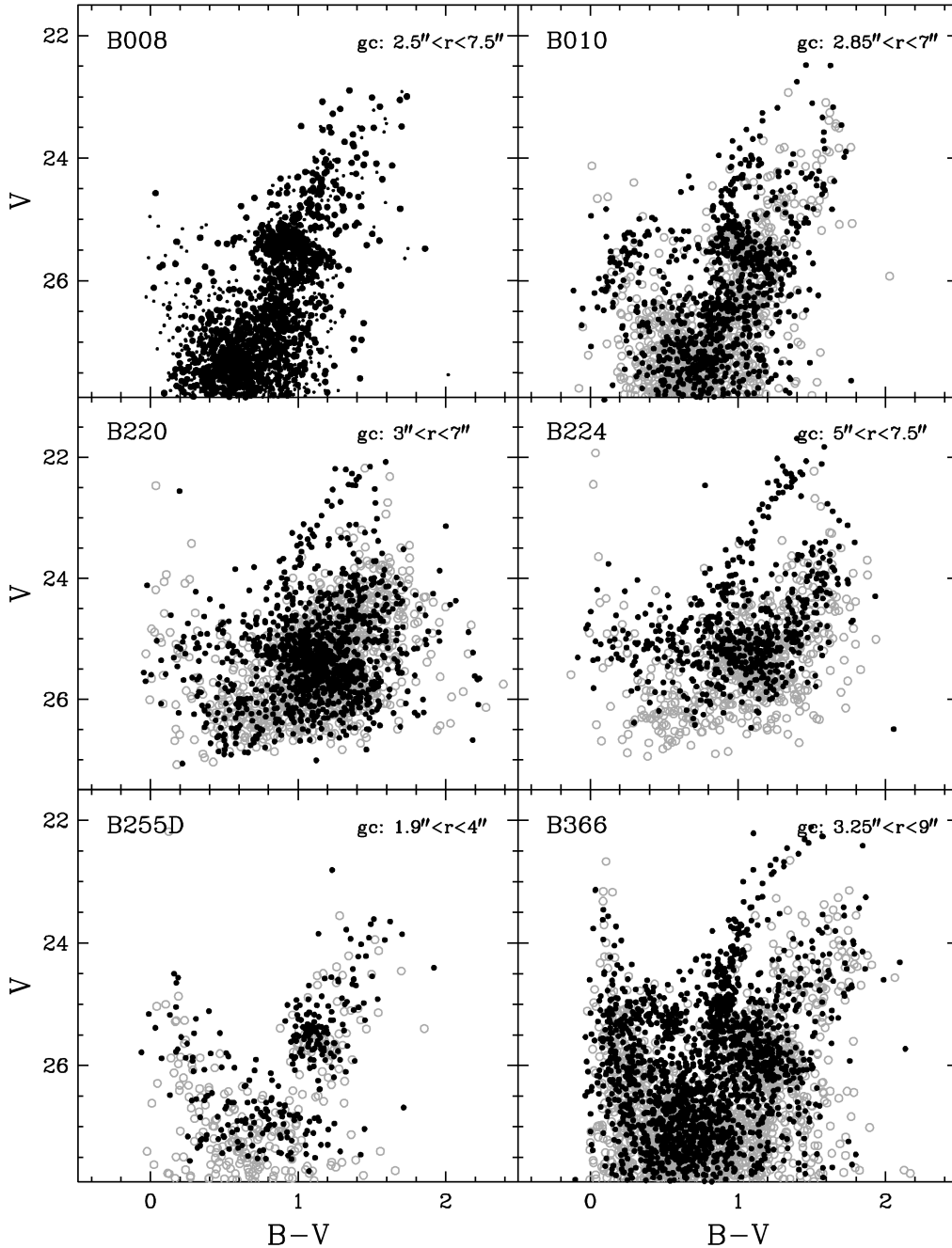


**Fig. 6.** The CMDs of the target GCs B008, B010, B220, B224, B255D, and B366. *Filled black circles* are stars measured within the annulus with radii  $r$  in arcsec from the cluster centre (as reported in each panel). They are taken to represent the cluster population; *open grey circles* are stars measured within an outer area, of the same size, around the cluster, and represent the surrounding field population.

satisfactory and reliable. We have explored also alternative solutions, some of which are discussed in Sect. 5. In all cases the final adopted solution was the one which provided the best fit for both RGB and HB simultaneously.

As a matter of fact, due to the intrinsic and well-known age-metallicity degeneracy, also age could be considered as an additional free parameter, which would further complicate the analysis, having a (minor) effect on the colour of the RGB. Since the data are not deep enough (i.e. to the main sequence turn-off) to allow us to estimate the cluster ages (for ages larger than

$\sim 2$  Gyr), we have assumed that all of the 11 primary target are classical old globulars (i.e. age  $> 10$  Gyrs). This assumption is supported by the overall morphology of the CMDs, in particular for those clusters displaying a Blue HB.

The best fitting procedure allowed us to estimate also the mean apparent  $V$  magnitude of the HB,  $V(\text{HB})$ , by reading the value of the HB apparent magnitude level directly on the *adopted HB ridge line* at  $(B-V)_0=0.3$  or  $(V-I)_0=0.5$  for the metal-poor clusters. This colour has been chosen to represent the middle of the instability strip. For the metal-rich clusters we have es-



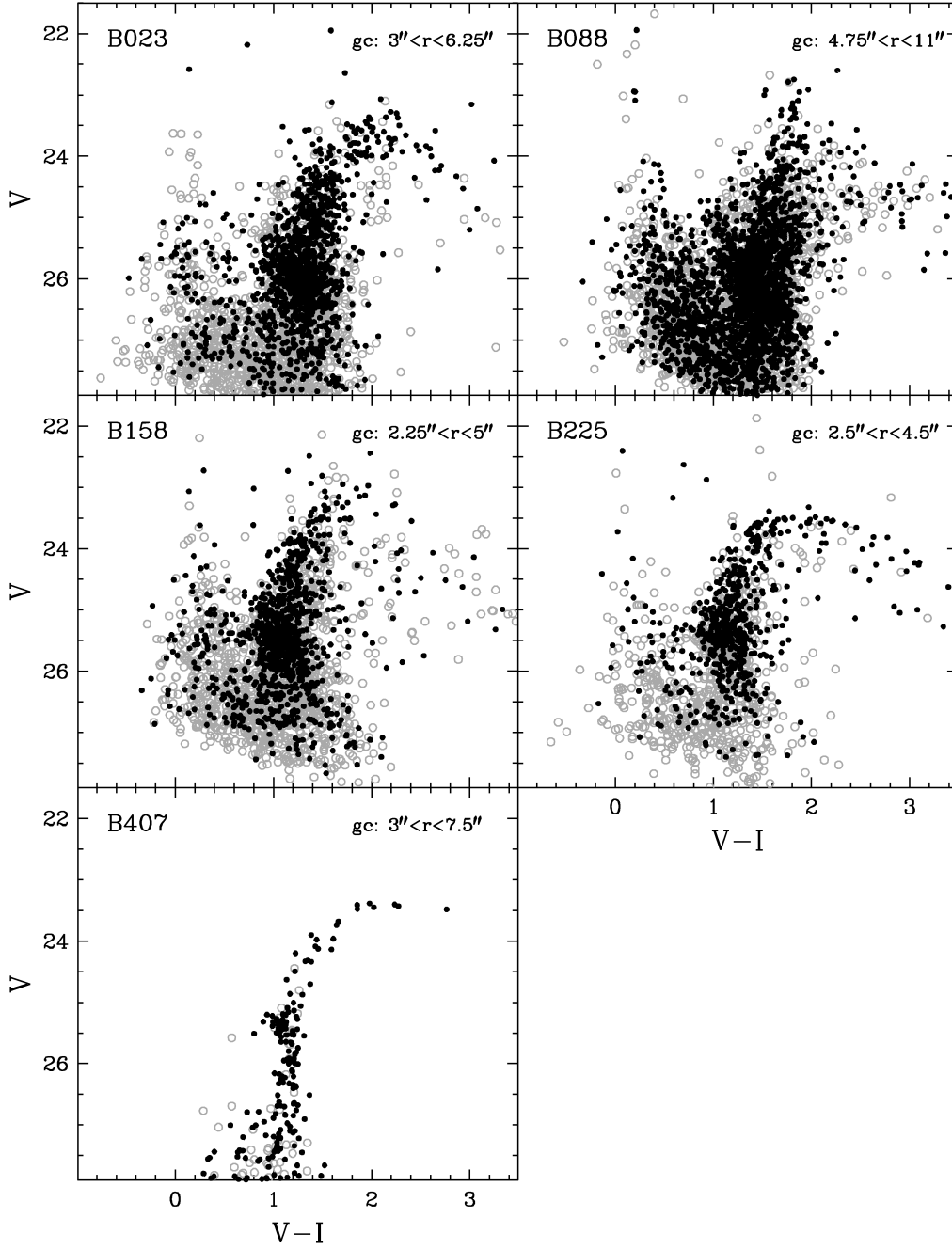


**Fig. 7.** Same as in Fig. 6 for the GCs B023, B088, B158, B225, and B407.

timated  $V(\text{HB})$  at the blue end of the red HB clump, with an additional correction of 0.08 mag to recover the mean level of the HB at the colour of the corresponding instability strip (see Fusi Pecci et al. 1996). The uncertainties affecting the  $V(\text{HB})$  estimates are often quite large, due to the intrinsic quality of the available data and the possible residual field contamination. We have conservatively adopted  $\pm 0.15$  mag for all the considered clusters.  $V(\text{HB})$  and  $M_V(\text{HB})$  are reported in Table 4, together with the other parameters derived from the above procedure.

In the following section we briefly discuss the cases of each individual cluster.

## 5. Comments on the individual clusters

### 5.1. B008 = G060

In spite of the strong field contamination the typical cluster morphology can be identified in the decontaminated CMD of B008. The cluster displays a red HB and an RGB falling about halfway between the ridge lines of 47 Tuc and M5, with no need of adjustment with respect to the initial assumptions on distance and reddening. This leads to estimate a metallicity  $[\text{Fe}/\text{H}] = -1.0 \pm 0.25$  (the error is the typical uncertainty in the interpolation between the bracketing ridge lines). This result is in marginal disagreement (at  $< 2\sigma$  level) with the estimates by Perrett et al. (2002, hereafter P02;  $[\text{Fe}/\text{H}] = -0.41 \pm 0.38$ ), and

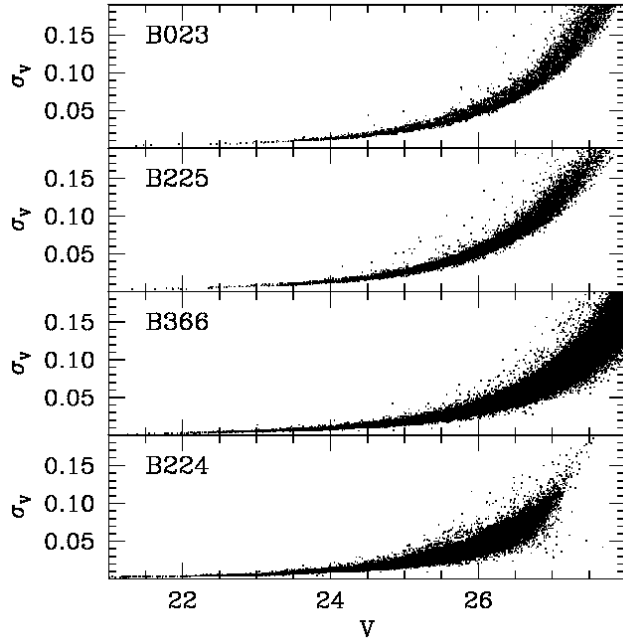


**Fig. 5.** Internal photometric errors as a function of  $V$  magnitude for 4 representative clusters, two observed with ACS/HRC (B225 and B023), and two observed with ACS/WFC (B224 and B366).

by Galleti et al. (2009, hereafter G09;  $[\text{Fe}/\text{H}] = -0.47 \pm 0.35$ ), both obtained from integrated ground-based spectroscopy. We collect in Table 5 all the available metallicity determinations for all the target clusters, for convenience of comparison with the present estimates. On the other hand, adopting the reddening  $E(B - V) = 0.21$  (as estimated by Barmby et al. 2000, and private communication, hereafter B00) an acceptable fit to the CMD morphology could only be obtained for  $\mu_0 = 24.20$  and  $[\text{Fe}/\text{H}] = -1.8$ , with even larger disagreement with the spectroscopic metallicity estimates. Although this solution cannot be excluded in principle, we consider it as highly unlikely, as our adopted best values provide a much better fit to the observed CMD.

### 5.2. B010 = G062

In this case, the decontaminated CMD is quite clean, showing a well defined and populated Blue HB and a steep RGB, indicating old age and low metal content. The best match of these features with the corresponding ridge lines is obtained by assuming a value of reddening  $E(B - V) = 0.18$  mag and a distance modulus  $\mu_0 = 24.25$ . The solution relies on the best match to the blue part of the HB, considering the handful of (supposed) HB stars around  $0.3 \lesssim (B - V)_0 \lesssim 0.5$  as *evolved* BHBs, i.e. post-ZAHB stars in their way to the Asymptotic Giant Branch (and hence brighter than the genuine unevolved HB stars that we are using as standard candles).

With these assumptions, the CMD shown in Fig. 9 indicates that the metallicity of B010 is very similar to NGC5824, namely  $[\text{Fe}/\text{H}] = 1.8 \pm 0.25$ . This value is in good agreement with the spectroscopic ground-based estimates,  $[\text{Fe}/\text{H}] = -1.87 \pm 0.61$  (Huchra et al. 1991, hereafter HBK),  $[\text{Fe}/\text{H}] = -1.77 \pm 0.14$  (P02), and  $[\text{Fe}/\text{H}] = -1.64 \pm 0.68$  (G09). Also the adopted reddening  $E(B - V) = 0.18$  is fully consistent with the values re-

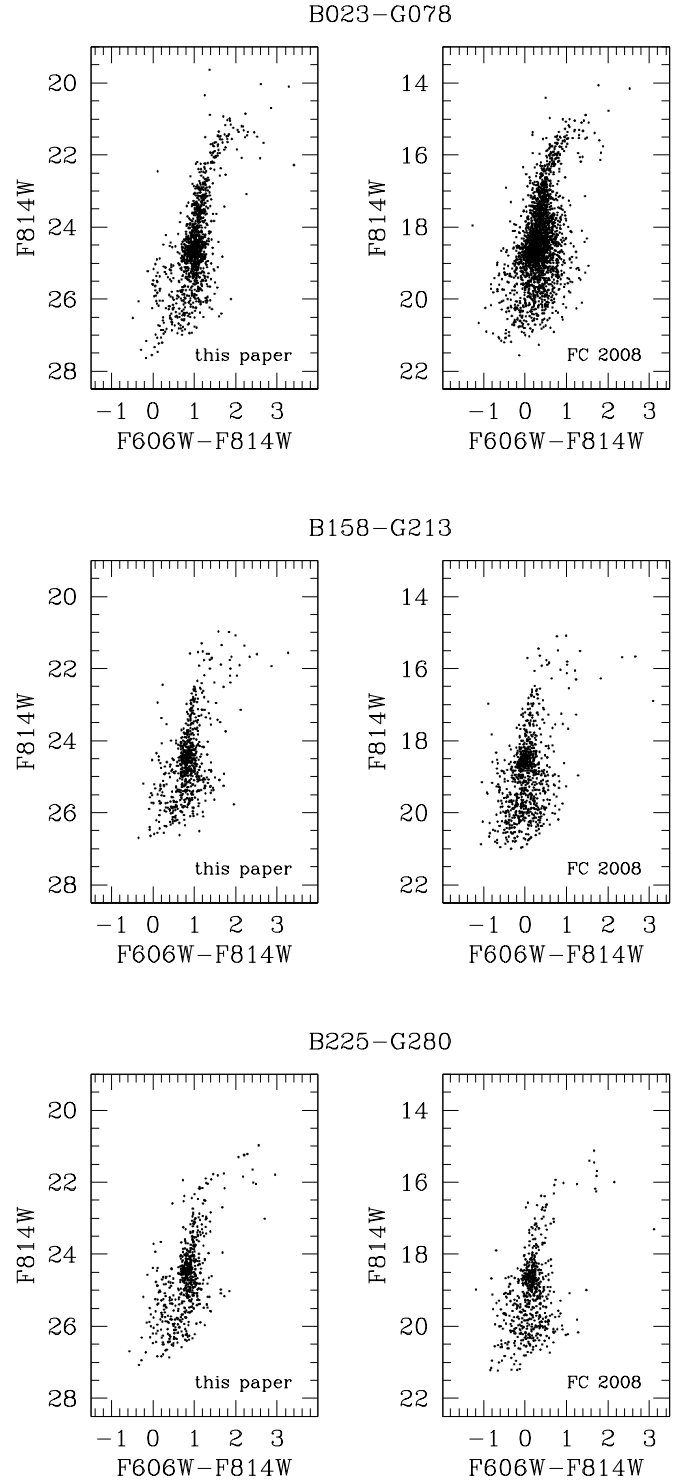


**Fig. 8.** Comparison of the CMDs obtained from the present study (left) and by Fuentes-Carrera et al. (2008, their Fig. 6) (right, uncalibrated VEGAMAG magnitudes), for the clusters B023 (top), B158 (middle) and B225 (bottom).

ported in the literature, i.e. 0.19 (B00) and 0.22 (Fan et al. 2008, hereafter F08).

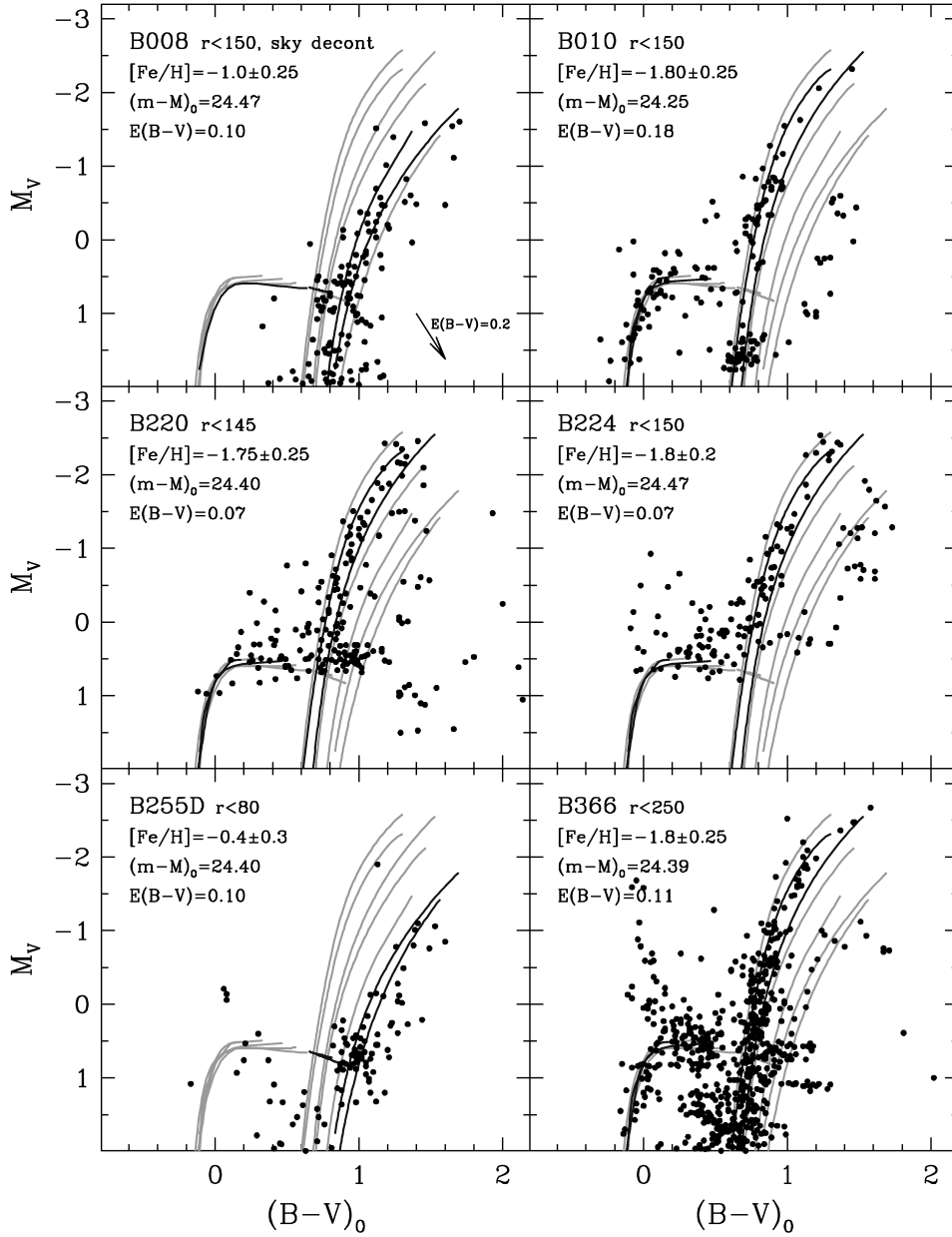


**Fig. 9.** The CMDs of the primary target GCs B008, B010, B220, B224, B255D and B366. The data have been decontaminated by the field contribution. The arrow in the left top panel indicates the reddening vector corresponding to  $e(B - V) = 0.2$ . The *bracketing ridge lines* of reference Galactic GCs are also shown, as described in Sect. 4 and Table 3.

### 5.3. B220 = G275

The CMD of B220 shows the presence of a well defined BHB and a rather steep RGB, indicating old age and a low metallicity content. The best match of these features of the CMD with the corresponding reference ridge lines is obtained by assuming a value of reddening  $E(B - V) = 0.07$  mag (in agreement with  $E(B - V) = 0.05$  by F08, and  $E(B - V) = 0.08$  by B00) and a distance modulus  $\mu_0 = 24.40$ . With these assumptions the CMD shown in Fig. 9 indicates that the metallicity of B220 is intermediate between M13 and NGC5824,  $[Fe/H] = -1.75 \pm 0.25$ . This value compares fairly well with the spectroscopic estimate

of HBK,  $[Fe/H] = -2.07 \pm 0.82$ , whereas the values found by P02,  $[Fe/H] = -1.21 \pm 0.09$  and G09  $[Fe/H] = -1.09 \pm 0.42$  seem too high for this cluster.

### 5.4. B224 = G279

The best match of the steep RGB and extended HB of B224 with the corresponding reference ridge lines is obtained by assuming a value of reddening  $E(B - V) = 0.07$  mag and the standard distance modulus of 24.47 mag. With these values, the CMD shown in Fig. 9 indicates that the metallicity of B224 is intermediate between M13 and NGC5824,  $[Fe/H] = -1.80 \pm 0.25$ . This value

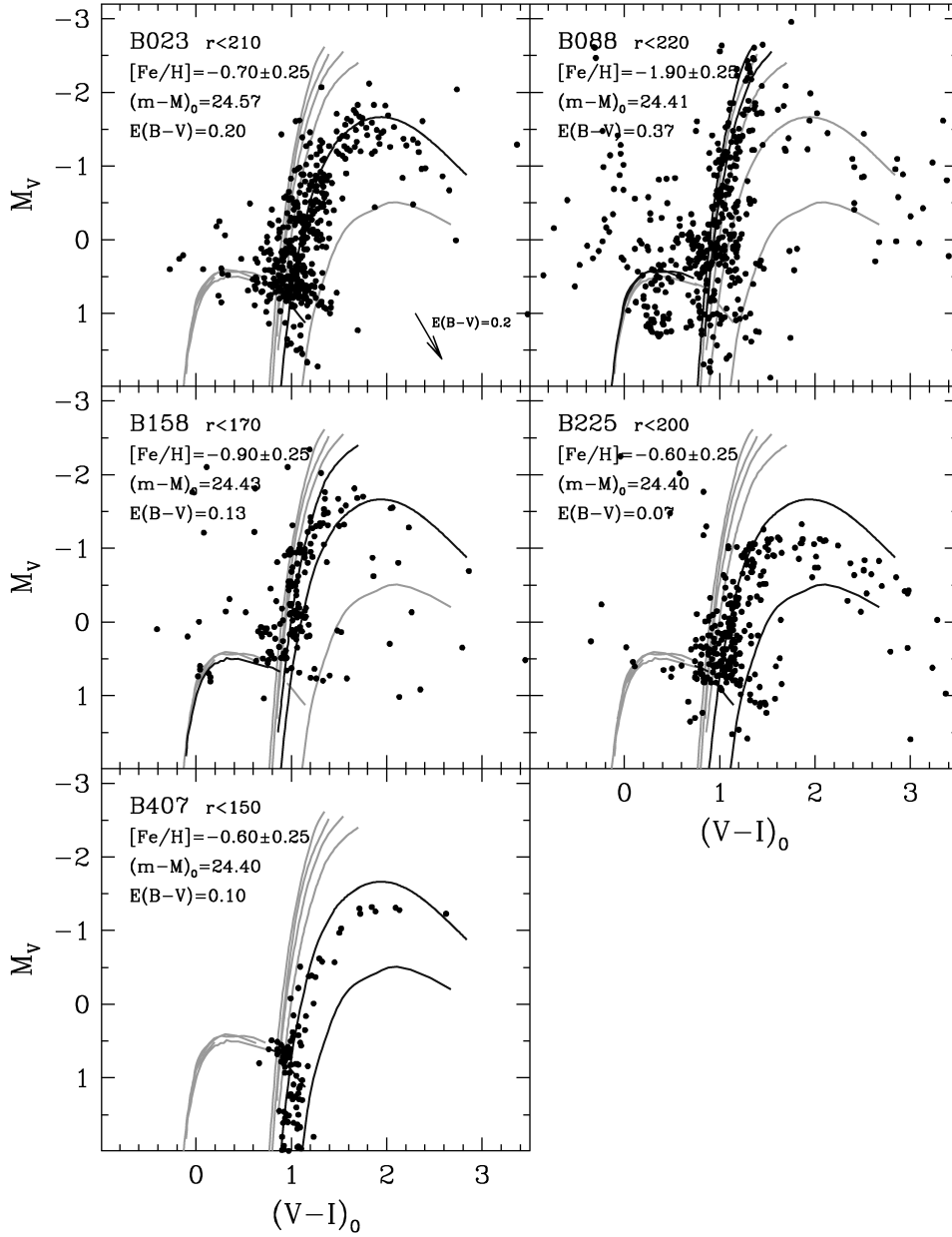


**Fig. 10.** Same as in Fig. 9 for the GCs B023, B088, B158, B225 and B407.

compares well with previous estimates from integrated spectroscopy:  $[\text{Fe}/\text{H}] = -1.90 \pm 0.24$  (HBK),  $[\text{Fe}/\text{H}] = -1.80 \pm 0.05$  (P02), and  $[\text{Fe}/\text{H}] = -1.68 \pm 0.28$  (G09).

Both F08 and B00 have estimated slightly higher reddening values: 0.13 and 0.12 mag, respectively. We have searched for solutions with  $E(B - V) = 0.13$ , and we found that the best fit would yield a similar metallicity but a much shorter distance,  $\mu_0 = 24.25$ . However, the overall quality of the fit is significantly worse when using this higher value of reddening, so we have adopted our primary solution.

### 5.5. B255D

The cluster is rather small and the statistical decontamination procedure becomes less effective when the number of stars is low. As a result, one can still see the presence of some residual field population on the blue side of the CMD (blue plume). Nevertheless, a sparse and metal-rich RGB as well as a red clump can be seen clearly. The best match with the ridge lines in this case is not much more than an intelligent guess, and indicates a metallicity  $[\text{Fe}/\text{H}] = -0.40 \pm 0.25$  and a distance modulus  $\mu_0 = 24.40$  mag for the assumed value of reddening  $E(B - V) = 0.10$  mag. There are no ground-based spectroscopic estimates for this cluster.

### 5.6. B366 = G291

B366 is a rather populous cluster lying in a high density field, as shown in Fig. 2. The decontamination procedure was not able to eliminate completely the field component (a blue plume as well as a red clump to the red of the cluster RGB), but the cluster population shows up quite clearly as a well defined HB with a possible blue extension, and a rather steep RGB, suggesting old age and metal deficiency. The cluster is classified as old also by C09, based on its integrated spectrum.

The best match between the observed CMD and the template ridge lines is achieved with  $E(B - V) = 0.11$  mag and  $\mu_0 = 24.39$  mag. With these values,  $[Fe/H] = -1.80 \pm 0.25$  is found. This value is consistent, within the uncertainties, with the spectroscopic estimates by HBK,  $[Fe/H] = -1.39 \pm 0.28$ , and G09,  $[Fe/H] = -2.14 \pm 0.39$ , while it is in excellent agreement with the results of P02,  $[Fe/H] = -1.79 \pm 0.05$ .

### 5.7. B023 = G078

The field decontamination has left some marginal field contribution on the bluest part of the CMD, but the main branches stand out quite clearly. The cluster has a red HB, and its RGB falls almost exactly on the ridge line of 47 Tuc.

The best match of the main branches is obtained for  $E(B - V) = 0.20$  mag and  $\mu_0 = 24.57$ . This leads to estimate a metallicity  $[Fe/H] = -0.70 \pm 0.25$ , in good agreement with existing spectroscopic estimates,  $[Fe/H] = -0.92 \pm 0.10$  by HBK, and  $[Fe/H] = -0.91 \pm 0.15$  by G09.

We note that the reddening estimated by Barmby et al. (2007, hereafter B07), and F08 is significantly larger,  $E(B - V) = 0.36$  and  $0.32$  mag, respectively. With these values no match can be achieved with any of the ridge lines, therefore we exclude the possibility of such a high reddening for this cluster.

### 5.8. B088 = G150

As one can see in Fig. 2, this cluster is very populous, has a strongly elliptical shape and lies in a rather dense field. Two other clusters in our sample, B023 and B366, show some evidence of elliptical shape, but the ellipticity of B088 is clearly larger. The values reported in the literature are  $\epsilon = 0.28$  (Barmby et al. 2007),  $\epsilon = 0.18$  (Staneva et al. 1996) and  $\epsilon = 0.23 - 0.27$  (Lupton 1989), making this object particularly noteworthy.

In this case, where the stellar field is very crowded and variable, we have performed several statistical field subtraction experiments. In spite of the presence of some residual contamination from the field, the steep cluster RGB is clearly identified in all cases, indicating a low metal content. On the other hand the HB morphology is more confused, and the vertical match is rather tentative. A possible adopted set of parameters is  $[Fe/H] = -1.90 \pm 0.25$ ,  $E(B - V) = 0.37$  and  $\mu_0 = 24.41$ . The metallicity agrees very well with spectroscopic estimates,  $[Fe/H] = -2.17 \pm 0.48$  (HBK),  $[Fe/H] = -1.81 \pm 0.06$  (P02), and  $[Fe/H] = -1.94 \pm 0.52$  (G09). A high value of reddening for this cluster was found independently by F08 (0.46 mag) and B07 (0.48 mag). Our result indicates that the cluster is located in the nearest side of the M31 disc, and lies behind some dust layer as clearly visible in the Spitzer images of this region (Gordon et al. 2006).

**Table 4.** Parameters derived for the 11 primary target clusters from the procedure described in Sect.s 4 and 5.

ID	$R_{HI}$ arcs	$V_{HB}$	$E(B-V)$	$\mu_0$	$[Fe/H]$ dex	$M_V^{HB}$ mag
B008-G60	0.95	25.29	0.10	24.47	$-1.00 \pm 0.25$	0.51
B010-G62	1.40	25.30	0.18	24.25	$-1.80 \pm 0.25$	0.49
B023-G78	0.95	25.91	0.20	24.57	$-0.70 \pm 0.25$	0.72
B088-G150	1.11	25.99	0.37	24.41	$-1.90 \pm 0.25$	0.43
B158-G213	0.65	25.44	0.13	24.43	$-0.90 \pm 0.25$	0.61
B220-G275	2.15	25.08	0.07	24.40	$-1.75 \pm 0.25$	0.46
B224-G279	1.35	25.22	0.07	24.47	$-1.80 \pm 0.25$	0.53
B225-G280	0.61	25.35	0.07	24.40	$-0.60 \pm 0.25$	0.73
B255D-D072	1.60	25.53	0.10	24.40	$-0.40 \pm 0.25$	0.82
B366-G291	2.00	25.25	0.11	24.39	$-1.80 \pm 0.25$	0.52
B407-G352	0.80	25.41	0.10	24.40	$-0.60 \pm 0.25$	0.70

### 5.9. B158 = G213

Even if sparsely populated, the steep RGB of B158 stands out quite clearly in the decontaminated CMD, while the fit to a (supposed) extended HB is just tentative. Our best solution gives an estimate of the reddening  $E(B - V) = 0.13$  mag, in excellent agreement with the results by F08,  $E(B - V) = 0.14$ , and B00,  $E(B - V) = 0.12$ . The adopted distance modulus is  $\mu_0 = 24.43$ , and the metallicity  $[Fe/H] = -0.90 \pm 0.25$ , which compares very well with all the ground-based estimates:  $[Fe/H] = -1.08 \pm 0.05$  (HBK),  $[Fe/H] = -1.02 \pm 0.02$  (P02), and  $[Fe/H] = -0.74 \pm 0.15$  (G09).

### 5.10. B225 = G280

The RGB and red HB of the cluster stand out very clearly and are well consistent with the ridge lines of the metal-richest templates, on the assumption of a reddening value  $E(B - V) = 0.07$  and a distance  $\mu_0 = 24.40$ . This leads to estimate a metallicity  $[Fe/H] = -0.60 \pm 0.25$ , in agreement with the spectroscopic estimates:  $[Fe/H] = -0.70 \pm 0.12$  (HBK),  $[Fe/H] = -0.67 \pm 0.12$  (P02), and  $[Fe/H] = -0.35 \pm 0.15$  (G09).

The CMD of this cluster was previously obtained by Fusi Pecci et al. (1996), with HST/FOC and, subsequently, by Rich et al. (2005), with HST/WFPC2. Both studies obtained results in good agreement with those presented here.

### 5.11. B407 = G352

The cluster B407 lies at a rather large projected distance from the centre of M31, in a low density region where the contamination by field stars is very low. As a consequence, the RGB and red HB of the cluster are very well defined. Their position in the CMD indicates a metallicity slightly higher than the reference cluster 47 Tuc.

The best solution is obtained for  $E(B - V) = 0.10$  mag and  $\mu_0 = 24.40$  mag. With these values, the metallicity of B407 is  $[Fe/H] = -0.60 \pm 0.25$ , fully consistent with the spectroscopic estimates by HBK,  $[Fe/H] = -0.85 \pm 0.33$  and, in particular, G09,  $[Fe/H] = -0.65 \pm 0.15$ .

The case of B407 as a metal rich cluster in the outer halo of M31 is discussed in more detail in Section 6.

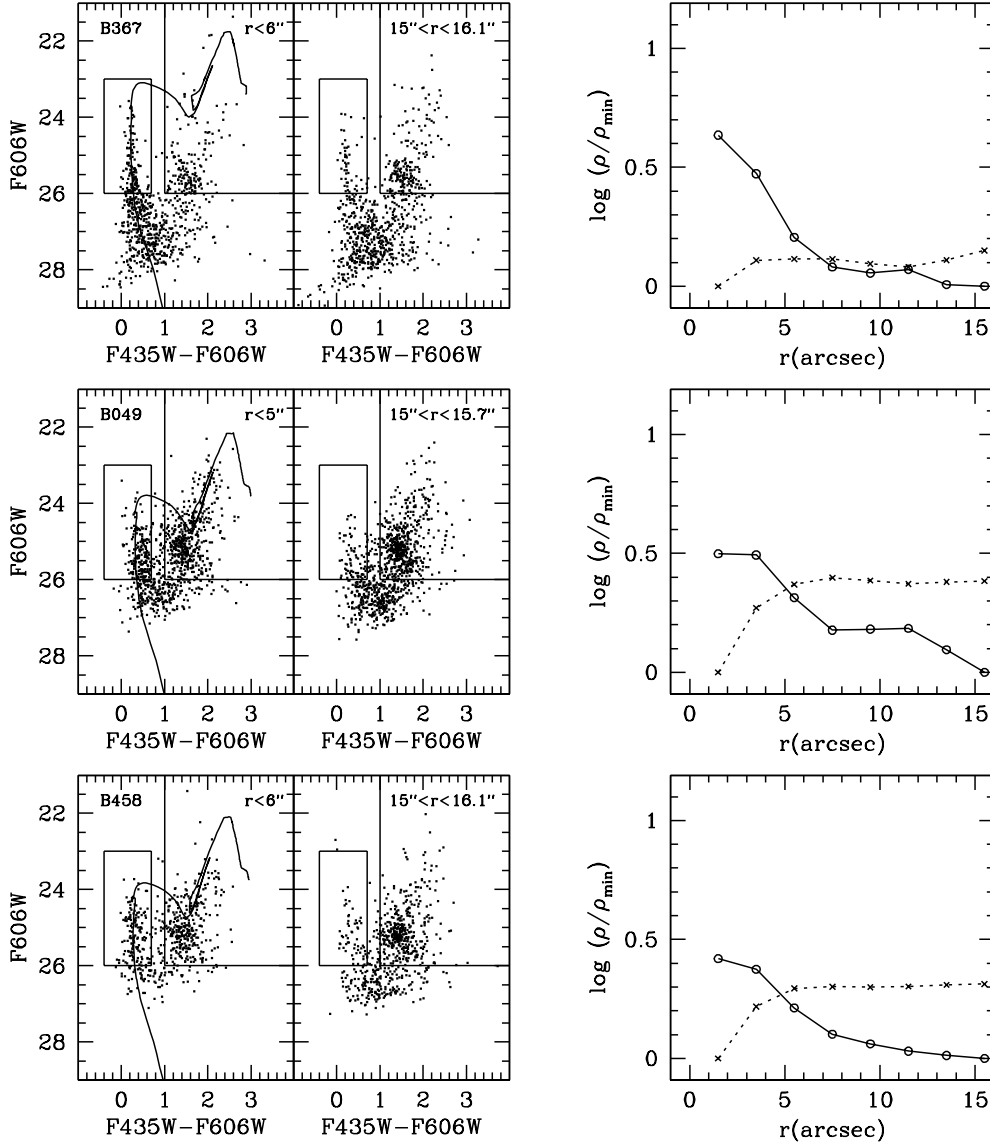


**Fig. 11.** *left:* CMDs of annuli dominated by the cluster population; *right:* CMDs of the surrounding fields, measured over annuli of similar area. Right panels report the radial profiles obtained by counting stars in the two boxes reported in the CMD plots. The *solid* lines show the radial behaviour of the “blue plume” in the smaller box, presumably including most of the cluster MS, while the *dotted* lines show the corresponding trend as obtained from the bigger boxes, presumably dominated by the field. Best-fitting isochrones with solar metallicity (Girardi et al. 2002) are overimposed.

### 5.12. The candidate young clusters

As noted in Sect.2, there are 9 clusters that we consider separately as they have been classified as young by previous studies. Five of them, namely B049, B057, B090, B367, B458, were included in the list of the so-called “Blue Luminous Compact Clusters” (BLCC, Fusi Pecci et al. 2005, F05 hereafter). They are quite faint,  $V \sim 17.5 - 18.5$ , but are undoubtedly clusters and some of them have the compact appearance that is typical of GCs (see Fig. 4; F05, Williams & Hodge 2001). B057 was included by F05 among the candidate “young” clusters due to the quite high  $H_\beta$ -value, 5.56, but C09 (see Table 6) classify it as “old” as well as B090, with a lower  $H_\beta$ -value, 3.38, that was included in the list of possible young candidates by Jiang et al. (2003).

Three other objects, B521, M050, M039 have been classified as “young” clusters by C09 (see Table 6). B521 is actually coincident with another object, SK034A, having measured ra-

dial velocity ( $v_r = -531.8 \text{ km s}^{-1}$ , Kim et al. 2007;  $v_r = -515.8 \text{ km s}^{-1}$ , C09). M050 is classified as a “young” cluster by C09 who found  $v_r = -156.6 \text{ km s}^{-1}$ . It looks like a small asymmetric aggregate of stars, but its CMD confirms that it is indeed a young cluster (see below). M039=KHM31-516 (Krienke and Hodge 2008) is faint and partially resolved, C09 list  $v_r = -82.4 \text{ km s}^{-1}$ . B515=KHM31-409 was listed by Krienke and Hodge (2008) as an open cluster<sup>4</sup>.

For 6 of the 9 clusters quoted above (B367, B049, B458, B521=SK034A, M039 and M050) we were able to obtain CMDs

<sup>4</sup> We note that another cluster of our sample, B041 (not considered in this section), that was classified as old by C09, was instead suggested to be young by Barmby et al. (2007). According to the latter study its red integrated colour is probably due to a red, bright, non-member star which masks the true intrinsic colour of the cluster. Unfortunately our data do not provide any further insight on the age of this cluster.



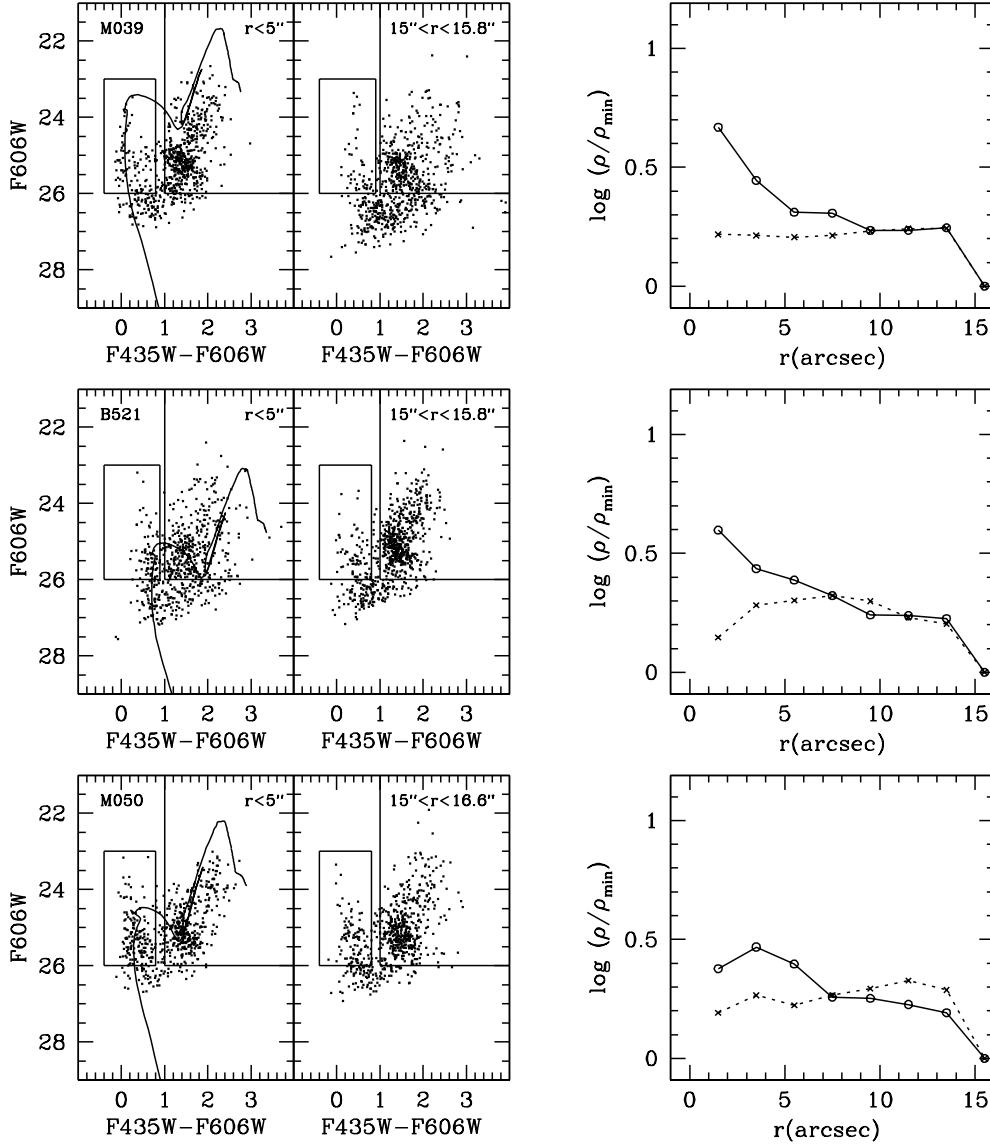


**Fig. 12.** Same as Fig. 11 for the clusters B521, M050 and M039.

representative of the cluster populations, that are shown in Figs. 11 and 12. On the rightmost panels of these figures we report the cluster density profiles obtained by counting stars on CMD boxes selecting the young main sequence (MS) population (open circles) and the red evolved population (RGB and Red Clump; crosses). Even if in most cases the CMD of the cluster is quite similar to that of the surrounding field (sampling the star-forming thin disc of M31), the density profiles show that in all cases a significant overdensity of MS stars is found at the cluster position. Guided by the density profiles we selected the radial annuli where the CMD is expected to be dominated by cluster stars (leftmost panels), to be compared with an external annulus of the same area sampling the surrounding field (central panels).

To have a rough estimate of the age and reddening, the CMDs of the clusters were fitted (by eye) with solar abundance isochrones (from Girardi et al. 2002), as done in Williams & Hodge (2001) and Perina et al. (2009a). The results, reported in Table 6, are in good agreement with similar estimates by C09 who adopted however super-solar abundance isochrones. All the six clusters for which the CMD could be derived (see Figs. 11

and 12) appear indeed younger than 1 Gyr, thus confirming their previous classification.

For the remaining three clusters B057, B090 and B515, it resulted impossible to single out the cluster population from the background, thus we cannot provide any improved age estimate.

It is worth noticing, that four of the clusters considered here (B367, B049, B458, and B057) have a spectroscopic metallicity estimate from P02 (see Tab. 2, above) that was obtained using a calibration that is based on (and valid only for) old clusters. Their high degree of metal deficiency reported by P02  $-1.18 < [Fe/H] < -2.32$  is very likely spurious, due to the known fact that a young age mimics the lack of metals in integrated colours and spectra (see Fusi Pecci et al. (2005) for a detailed discussion of this effect in the context of the study of the GC system of M31). Moreover, in a search for groups of M31 GCs having common origin (from the disruption of the same parent dwarf galaxy, for instance) based on the similarity in position, velocity, and metallicity, Perrett et al. (2003) identified eleven remarkable groups. Their group 9 contains B049 and B458, confirmed here as having age  $< 1$  Gyr from their CMD, B057 and DAO408, classified as young from their  $H_{\beta}$  and/or

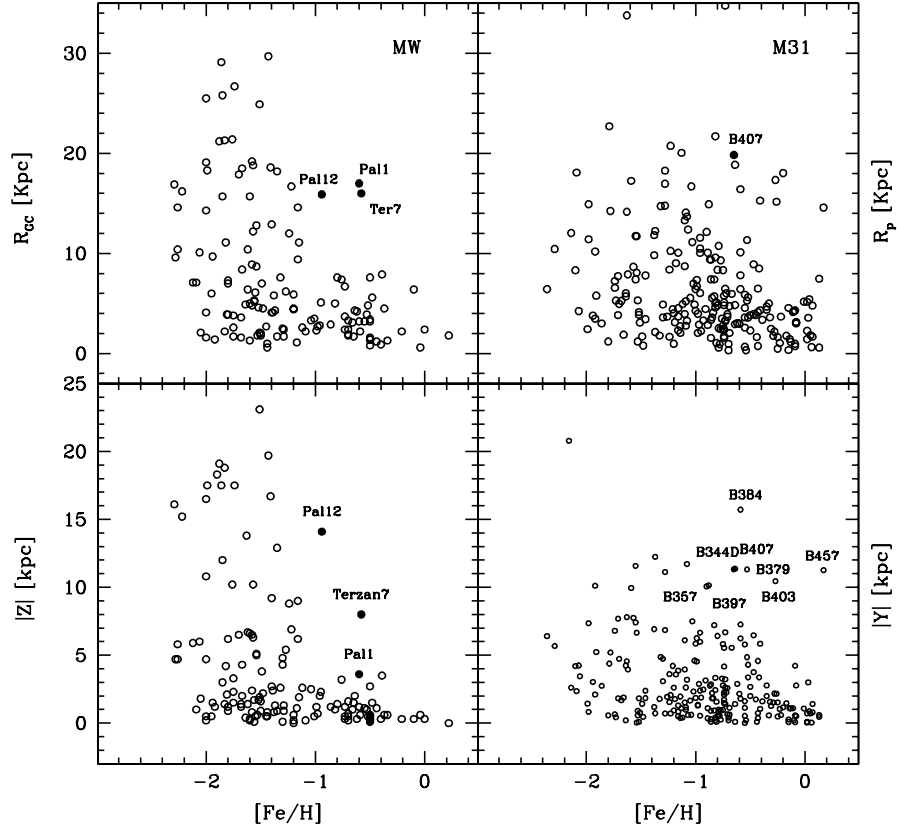


**Fig. 13.** Left panels: distribution of Galactocentric distance (upper-left) and absolute height above the Galactic plane (lower-left) as a function of metallicity for Galactic GCs (from Harris 1996). The clusters having  $[\text{Fe}/\text{H}] \geq -1.0$  and  $R_{GC} > 10$  kpc are plotted as filled circles and labelled with their names. Right panels: projected M31 galactocentric distance (upper-right) and projected distance from the major-axis (lower-right) as a function of metallicity for M31 CGs (from G09). B407, as well as other clusters having  $[\text{Fe}/\text{H}] \geq -1.0$  and unusually high  $Y$ , are labelled with their names, B407 is highlighted as a filled circle.

**Table 5.** Comparison of the estimates of metallicity here obtained for the target clusters (see Sect.s 4 and 5) and previous recent determinations.

ID	$[\text{Fe}/\text{H}]_{\text{CMD}}$ dex	$[\text{Fe}/\text{H}]_{\text{G09}}$ dex	$[\text{Fe}/\text{H}]_{\text{P02}}$ dex	$[\text{Fe}/\text{H}]_{\text{HBK}}$ dex
B008-G60	$-1.00 \pm 0.25$	$-0.47 \pm 0.35$	$-0.41 \pm 0.38$	
B010-G62	$-1.80 \pm 0.25$	$-1.64 \pm 0.68$	$-1.77 \pm 0.14$	$-1.87 \pm 0.61$
B023-G78	$-0.70 \pm 0.25$	$-0.91 \pm 0.15$		$-0.92 \pm 0.10$
B088-G150	$-1.90 \pm 0.25$	$-1.94 \pm 0.52$	$-1.81 \pm 0.06$	$-2.17 \pm 0.48$
B158-G213	$-0.90 \pm 0.25$	$-0.74 \pm 0.15$	$-1.02 \pm 0.02$	$-1.08 \pm 0.05$
B220-G275	$-1.75 \pm 0.25$	$-1.09 \pm 0.42$	$-1.21 \pm 0.09$	$-2.07 \pm 0.82$
B224-G279	$-1.80 \pm 0.25$	$-1.68 \pm 0.28$	$-1.80 \pm 0.05$	$-1.90 \pm 0.24$
B225-G280	$-0.60 \pm 0.25$	$-0.35 \pm 0.15$	$-0.67 \pm 0.12$	$-0.70 \pm 0.12$
B255D-D072	$-0.40 \pm 0.25$			
B366-G291	$-1.80 \pm 0.25$	$-2.14 \pm 0.39$	$-1.79 \pm 0.05$	$-1.39 \pm 0.28$
B407-G352	$-0.60 \pm 0.25$	$-0.65 \pm 0.15$		$-0.85 \pm 0.33$

CMD: this paper; G09: (Galletti et al. 2009); P02: Perrett et al. (2002); HBK: Huchra et al. (1991).

**Table 6.** Parameters derived for the candidate young clusters. Photometry is from G04 except when otherwise stated.  $R_{hl}$  indicates the half-light radius.

ID	$R_{hl}$ (arcs)	V	(B-V)	$E(B-V)$	Age (Myr) (this paper)	$E(B-V)$	Age (Myr) (C09)
B049-G112	1.20	17.56	0.52	0.30	280	0.25	400
B090	0.47	18.80					old
B367-G292	0.94	18.45	0.32	0.25	200	0.25	200
B458-D049	1.60	17.84	0.49	0.25	320	0.25	500
B515	1.25	18.60 <sup>1</sup>					
B521-SK034A	0.75	19.08 <sup>1</sup>		0.55	400	0.38	250
M039	0.62	18.94		0.10	320	0.18	320
M050	0.80	18.71		0.15	560	0.25	300
B057-G118	0.70	17.64	0.69				old

(<sup>1</sup>): V magnitude from C09.

colour in the RBC, and B034. Thus, four of the five members of the group are young clusters having velocities in full agree-

ment with the overall rotation pattern of M31 disc. As they likely belong to the disc, their proximity in space naturally implies similar velocities, while the similarity in metallicity is due to their

young age being mis-interpreted as low metal content, as described above. We conclude that this proposed group does not trace a real overdensity in the phase-space of the M31 halo, but simply a bunch of bright young disc clusters lying in the same spot of the disc.

A thorough discussion of "young" and bright clusters in M31 with HST-based CMDs, based on a wide homogeneous sample of other 18 candidates (P.I. J. Cohen GO 10818) and also including the six clusters studied here and the four clusters by Williams and Hodge (2001), will be presented in a forthcoming paper (see Perina et al. 2009a, for a presentation of the overall project). For a discussion about faint young clusters in M31 we refer the reader to Krienke and Hodge (2007, 2008).

## 6. Clusters in Streams

Among all the clusters of our sample, B407 is the most distant from the centre of M31, lying at a projected distance of about 20 kpc. It is also one of the most metal rich, and this combination makes it worth a more detailed investigation.

In Fig. 13 we show the distribution of Galactocentric distance and absolute height above the Galactic plane as a function of metallicity for GCs in the Milky Way (from Harris 1996). It is quite clear that, while metal-poor clusters ( $[\text{Fe}/\text{H}] \lesssim -1$ ) are found at any  $R_{GC}$  and/or  $|Z|$ , the metal-rich ( $[\text{Fe}/\text{H}] \gtrsim -1$ ) clusters are confined within  $R_{GC} < 8$  kpc and  $|Z| < 3$  kpc<sup>5</sup>. The only exceptions are three metal-rich clusters that do not satisfy these conditions and stand out as obvious outliers in Fig. 13, namely Terzan 7, Palomar 12 and Palomar 1. Ter 7 is a member of the Sagittarius dwarf spheroidal galaxy (Ibata et al. 1994, 1995), a satellite of the MW that is currently disrupting under the strain of the Galactic tidal field. In this process it has developed two huge tidal tails (Sgr Stream) containing its former stars (Ibata et al. 2001a; Majewski et al. 2003; Belokurov et al. 2006) and clusters (Bellazzini et al. 2003a) escaped during various perigalactic passages. Pal 12 is indeed associated with the Sgr Stream (Dinescu et al. 2000; Martinez-Delgado et al. 2002; Bellazzini et al. 2003a,b; Cohen 2004). An extra-galactic origin has been invoked also for Pal 1, to explain its anomalously young age (Rosenberg et al. 1998) and its unusual abundance pattern (Venn et al. 2007; Correnti, Saviane & Monaco, private communication). These characteristics are shared also by Ter 7 (Buonanno et al. 1995; Tautvaisiené et al. 2004; Sbordone et al. 2005) and Pal 12 (Stetson et al. 1989; Brown et al. 1997; Cohen 2004). The recent extensive and homogeneous analysis of relative ages of Galactic GCs by Marin-Franch et al. (2009) identifies Pal 1, Pal 12 and Ter 7 as the three youngest clusters of their whole sample. In conclusion, the diagrams in the left panels of Fig. 13 are very effective in identifying as outliers three clusters that are (most likely) of extra-galactic origin.

In the right panels of Fig. 13 we show the similar kind of plots for the M31 GCs (metallicities from G09). Unfortunately, in the case of M31 we have at disposal only projected quantities (the projected galactocentric distance  $R_p$ , and the projected distance from the major axis, a proxy for the height above the disc), unavoidably blurring the information contained in their de-projected counterparts. Nevertheless, the overall morphology of the distributions is quite similar to the MW case. In particular

<sup>5</sup> Incidentally, we note that the transition between the clusters confined to low  $R_{GC}$  and  $|Z|$  and those distributed over the whole range spanned by these parameters seems to be *very sharp*, occurring nearly exactly at  $[\text{Fe}/\text{H}] = -1.2$ .

there is just a bunch of metal-rich clusters having large  $R_p$  and  $Y$ , including B407.

To see if the anomaly in the position of these clusters can be traced also in their kinematics, in Fig. 14 we plot the projected position of metal-rich ( $[\text{Fe}/\text{H}] \geq -1.0$ ) clusters in the plane of the sky (upper panel), and their M31-centric radial velocity as a function of their distance along the major axis (assuming  $V_{r,0} = -301$  km/s as the systemic velocity of M31, Van den Bergh 2000). It is well known that, at odds with the MW case, the bulk of M31 GCs participate to the rotation pattern of the galaxy disc, as traced by the HI rotation curve, and the correlation is tighter for metal-rich clusters (P02; Lee et al. 2008; G09, and references therein). Among the clusters labelled in Fig. 13 as having an anomalous position for their metallicity, three have velocities in stark contrast with the rotation pattern shared by the bulk of the metal-rich GCs: B357, B403 and B407. In particular, the latter two clusters lie within a projected distance of 3 kpc from each other, and have velocities differing by  $\approx 20$  km/s. It is tempting to suggest that the two clusters are (were) physically associated to a common structure, having a different origin from the bulk of the other clusters. Recent extensive surveys have revealed that the halo and the outer disc of M31 host a wealth of sub-structures, generally believed to be the relics of past accretion events that contributed to the build-up of the galaxy (Ibata et al. 2001b, 2005, 2007; Ferguson et al. 2005).

Indeed, the CMD of B407 presented here has been obtained from an image of the set used by Richardson et al. (2008) to study the field stellar population within the main sub-structures identified in Ferguson et al. (2005) and Ibata et al. (2007). In particular, the cluster is at the edge of an ACS image sampling the so called NE Shelf, a thin stream of stars looping over the North-Eastern edge of the M31 disc. Richardson et al. find that the structure is mainly composed by stars with metallicity similar to what we find for B407, also very similar to the population found in the largest structure identified by Ferguson et al. (2005) and Ibata et al. (2007), i.e. the "Giant Stream". Ibata et al. (2005) studied the kinematics of stars in a field of the NE Shelf not far from B407/B403. They find a bimodal  $V_r$  distribution with a major peak at the characteristic velocity of the M31 disc at this position ( $V_r \sim -200$  km/s), and a secondary peak at  $V_r \sim -350$  km/s. We note that the velocities of the considered clusters match pretty well the secondary peak ( $V_r = -338, -358$  km/s for B407, B403 respectively), supporting the hypothesis of physical association with the component of field stars that do not follows the kinematics of the disc.<sup>6</sup>

The case described here opens a new window for the research of substructures in M31, as it shows that it may be possible to use GCs to trace (and easily study the kinematics) of at least some of the relics of past accretion events (see also Lee et al. 2008). It also supports the idea that the ingestion of GCs from accreting dwarf galaxies may provide a significant contribution to the assembly of the globular cluster systems of giant galaxies, as already shown in the case of the Milky Way (Bellazzini et al. 2003b)

## 7. Summary and conclusions

We have analysed 63 objects listed in the RBC for which HST/ACS images were publicly available in the HST Archive. We have confirmed or revised their classification based on the in-

<sup>6</sup> Another cluster, B401, having very similar position and velocity ( $X = 56.99, Y = -32.30, V_r = -333$  km/s), was not plotted in Fig. 14 because of its very low metallicity ( $[\text{Fe}/\text{H}] = -2.03$ ).

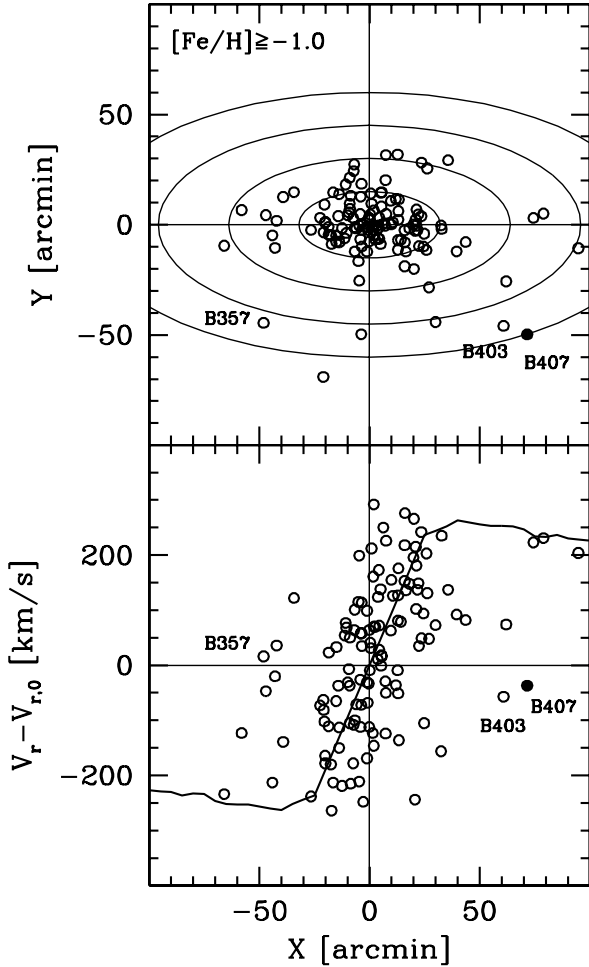


**Fig. 14.** Upper panel: X,Y distribution of M31 GCs having  $[\text{Fe}/\text{H}] \geq -1.0$ . The ellipses overplotted have major axes of  $30'$ ,  $60'$ ,  $90'$  and  $120'$ , respectively, and have the same axis-ratio and orientation as the disc of M31. Lower panel: Radial velocity as a function of major-axis distance for the same M31 GCs as above. The line is the HI rotation curve of the galaxy from Carignan et al. (2006). We have labelled only the clusters, among those labelled in Fig. 13, that do not follow the general rotation pattern.

spection of these images and we were able to obtain meaningful CMD for 11 likely old GCs and 6 young bright clusters.

We estimated distance, reddening, and metallicity for the eleven old GCs, by comparing the field-decontaminated CMD of the clusters with a grid of ridge lines of well-studied template clusters of the Milky Way. Our reddening and metallicity estimates are, in general, in satisfactory agreement with previous independent measures. As reported in Table 4, we have also determined for each cluster an estimate of the magnitude level of the HB measured on the HB ridge line of the reference GC that best fits the observed CMD, with a typical error of  $\pm 0.15$  mag.

One of the clusters of our sample (B407) is identified as a possible member of a large sub-structure recently found in the halo of M31, and interpreted as a relic of past (minor) merging episodes (NE Shelf; Ibata et al. 2001b, 2005, 2007; Richardson et al. 2008). The cluster has a metallicity that is much higher than the bulk of M31 clusters residing at the same (large) distance from the M31 centre/major axis, and its kinematics is very different from the large majority of M31 GCs having similar metallicity. The GC B403 (not included in our sample) is found

to share the same properties and is also indicated as a possible member of the NE Shelf.

We estimated the age also for six candidate young clusters, by comparing their observed CMD with theoretical isochrones. We confirm that all of them are younger than 1 Gyr, in good agreement with previous studies.

With the present analysis the total number of M31 confirmed GCs with published reliable optical CMDs increases from 35 to 44 for the old globulars, and from 7 to 11 for the young bright ones (BLCCs). The photometric catalogues of the clusters studied here will be made publicly available through a dedicated web page<sup>7</sup>.

*Acknowledgements.* We are grateful to P. Barmby for providing her unpublished list of reddening estimates for M31 GCs. We thank the referee, M. Rich, for useful comments and suggestions. This research was supported by ASI through the grant I/023/05/0. S.P., M.B. and C.C. acknowledge the financial support by INAF under the PRIN 2007 grant CRA 1.06.10.04.

## References

- Ajhar, E. A., Grillmair, C. J., Lauer, T. R., Baum, W. A., et al. 1996, *AJ*, 111, 1110
- Barmby, P., Huchra, J. P., Brodie J. P., Forbes, D. A., Schroder, L. L., & Grillmair, C. J. 2000, *AJ*, 119, 727 [B00]
- Barmby, P., McLaughlin, D.E., Harris, W.E., & Harris, G.L.H. 2007, *AJ*, 133, 2764 [B07]
- Bellazzini, M., Ferraro, F. R., & Buonanno, R. 1999, *MNRAS*, 304, 633
- Bellazzini, M., Ibata, R., Ferraro, F. R., & Testa, V. 2003a, *A&A*, 405, 577
- Bellazzini, M., Ferraro, F. R., & Ibata, R. 2003b, *AJ*, 125, 188
- Belokurov, V., Zucker, D. B., Evans, N. W., Gilmore, G., Vidrih, S., et al. 2006, *ApJ*, 642, L137
- Brown, J. A., Wallerstein, G., & Zucker, D. 1997, *AJ*, 114, 180
- Brown, T.M., Ferguson, H.C., Smith, E., Kimble, R.A., Sweigart, A.V., Renzini, A., Rich, R.M. & VandenBerg, D.A. 2004, *ApJ*, 613, L125
- Buonanno, R., Corsi, C.E., Pulone, L., Fusi Pecci, F., Richer, H.B., Fahlman, G.C. 1995, *AJ*, 109, 663
- Burstein D., Heiles C. 1984, *ApJS*, 54, 33
- Caldwell, N., Harding, P., Morrison, H., Rose, J.A., Schiavon, R., Kriessler, J. 2009, *AJ*, 137, 94 [C09]
- Carignan, C., Chemin, L., Huchtmeier, W.K., Lockman, F.J. 2006, *ApJ*, 641, L109
- Cohen, J.G. 2004, *AJ*, 127, 1545
- Dinescu, D.I., Majewski, S.R., Girard, T.M., & Cudworth, K.M. 2000, *AJ*, 120, 1892
- Dolphin, A.E. 2000a, *PASP*, 112, 1383
- Dolphin, A.E. 2000b, *PASP*, 112, 1397
- Fan, Z., Ma, J., deGrijs, R. and Zhou, X. 2008, *MNRAS*, 385, 1973 [F08]
- Ferguson, A.M.N., Johnson, R.A., Faria, D.C., Irwin, M.J., Ibata, R.A., Johnston, K.V., Lewis, G.F., & Tanvir, N.R. 2005, *ApJ*, 622, L109
- Fuentes-Carrera, I.; Jablonka, P.; Sarajedini, A.; Bridges, T.; Djorgovski, G.; Meylan, G. 2008, *A&A*, 483, 769 [FC08]
- Fusi Pecci, F., Buonanno, R., Cacciari, C., Corsi, C.E., Djorgovski, S.G., Federici, L., Ferraro, F.R., Parmegiani, G., Rich, R.M. 1996, *AJ*, 112, 1461
- Fusi Pecci, F., Bellazzini, M., Buzzoni, A., De Simone, E., Federici, L. & Galletti, S. 2005, *AJ*, 130, 554 [F05]
- Galletti, S., Federici, L., Bellazzini, M., Fusi Pecci, F. & Macrino, S. 2004, *A&A*, 416,917 (G04)
- Galletti, S., Federici, L., Bellazzini, M., Buzzoni, A. & Fusi Pecci, F. 2006a, *A&A*, 456, 985
- Galletti, S., Federici, L., Bellazzini, M., Buzzoni, A. & Fusi Pecci, F. 2006b, *ApJ*, 650, L107
- Galletti, S., Bellazzini, M., Federici, L., Buzzoni, A. & Fusi Pecci, F. 2007, *A&A*, 471, 127
- Galletti, S., et al. 2009, *A&A*, in press [G09]
- Girardi, L., Bertelli, G., Bressan, A., et al. 2002, *A&A*, 391, 195
- Gordon, K.D., Bailin, J., Engelbracht, C.W., Rieke, G.H., Misselt, K.A. and 14 coauthors 2006, *ApJ*, 638, L92
- Harris, W.E. 1996, *AJ*, 112, 1487
- Harris, W.E. 2003, Catalog of parameters for Milky Way Globular Clusters, Feb. 2003 update at <http://physwww.mcmaster.ca/~harris/mwgc.dat>
- Holland, S., Fahlman, G.G., Richer, H.B. 1997, *AJ*, 114, 1488

<sup>7</sup> <http://www.bo.astro.it/M31/hstcatalog>

- Huchra, J.P., Brodie, J.P., & Kent, S.M. 1991, *ApJ*, 370, 495 [HBK]
- Huxor, A., Tanvir, N.R., Irwin, M.J., Ferguson, A., et al. 2004, in *Satellites and Tidal Streams*, Eds. F. Prada, D. Martínez-Delgado, and T.J. Mahoney, ASP Conf Ser. Vol. 327, p. 118
- Huxor, A., Tanvir, N.R., Irwin, M.J., Ibata, R., et al. 2005, *MNRAS*, 360, 1007
- Huxor, A., Tanvir, N.R., Ferguson, A.M.N., Irwin, M., et al. 2008, *MNRAS*, 385, 1989
- Kim, S.C., Lee, M.G., Geisler, D., Sarajedini, A., Park, H.S. et al. 2007, *AJ*, 134, 706
- Krienke, O.K., & Hodge, P.W. 2007, *PASP*, 119, 7
- Krienke, O.K., & Hodge, P.W. 2008, *PASP*, 120, 1
- Ibata, R.A., Gilmore, G., Irwin, M.J. 1994, *Nature*, 370, 194
- Ibata, R.A., Gilmore, G., Irwin, M.J. 1995, *MNRAS*, 277, 781
- Ibata, R., Irwin, M., Lewis, G.F., Stolte, A. 2001a, *ApJ*, 547, L133
- Ibata, R., Irwin, M., Lewis, G., Ferguson, A.M.N., Tanvir, N. 2001b, *Nature*, 412, 49
- Ibata, R., Chapman, S., Ferguson, A.M.N., Lewis, G., Irwin, M., Tanvir, N. 2005, *ApJ*, 634, 287
- Ibata, R., Martin, N.F., Irwin, M., Chapman, S., Ferguson, A.M.N., Lewis, G.F., & McConnachie, A. W. 2007, *ApJ*, 671, 1591
- Jablonka, P., Courbin, F., Meylan, G., Sarajedini, A., Bridges, T.J. & Magain, P. 2000, *A&A*, 359, 131
- Jiang, L., Ma, J., Zhou, X., Chen, J., Wu, H., et al. 2003, *AJ*, 125, 727
- Lee, M. G., Hwang, H.S., Kim, S.C., Park, H.S., Geisler, D., Sarajedini, A., Harris, W.E. 2008, *ApJ*, 674, 886
- Lupton, R.H. 1989, *AJ*, 97, 1350
- Mackey, A.D., Huxor, A., Ferguson, A.M.N., Tanvir, N.R. et al. 2006, *ApJ*, 653, L105
- Mackey, A.D., Huxor, A., Ferguson, A.M.N., Tanvir, N.R. et al. 2007, *ApJ*, 655, L85
- Majewski, S.R., Skrutskie, M.F., Weinberg, M.D., & Ostheimer, J.C. 2003, *ApJ*, 599, 1082
- Marin-Franch, A., Aparicio, A., Piotto, G., Rosenberg, A., Chaboyer, B. et al. 2009, *ApJ*, 694, 1498
- Martin, N.F., Ibata, R.A., Irwin, M.J., Chapman, S., Lewis, G. F., et al. 2006, *MNRAS*, 371, 1983
- Martinez-Delgado, D., Zinn, R., Carrera, R., & Gallart, C. 2002, *ApJ*, 537, L19
- McConnachie, A.W., Irwin, M.J. & Ferguson, A.M.N. 2005, *MNRAS*, 356, 979
- Meylan, G., Sarajedini, A., Jablonka, P., Djorgovski, S.G., Bridges, T., Rich, R.M. 2001, *AJ*, 122, 830
- Perina, S., Barmby, P., Beasley, M.A., Bellazzini, M., Brodie, J.P., and 10 coauthors 2009a, *A&A*, 494, 933
- Perina et al. 2009b, in preparation
- Perrett, K.M., Bridges, T.J., Hanes, D.A., Irwin, M. J., Brodie, J. P., Carter, D., Huchra, J. P., Watson, F. G. 2002, *AJ*, 123, 2490 [P02]
- Perrett, K.M., Stiff, D.A., Hanes, D.A., & Bridges, T.J. 2003, *ApJ*, 589, 790
- Piotto, G., King, I.R., Djorgovski, S.G., Sosin, C., Zoccali, M. et al. 2002, *A&A*, 391, 945
- Puzia, T.H., Perrett, K.M., Bridges, T.J. 2005, *A&A*, 434, 909
- Rich, R.M., Mighell, K.J., Freedman, W., & Neill, J.D. 1996, *AJ*, 111, 768
- Rich, R.M., Corsi, C.E., Cacciari, C., Federici, L., Fusi Pecci, F., Djorgovski, S.G. & Freedman, W.L. 2005, *AJ*, 129, 2670
- Richardson, J.C., Ferguson, A.M.N., Johnson, R.A., Irwin, M.J., Tanvir, N.R., Faria, D.C., Ibata, R.A., et al. 2008, *AJ*, 135, 1998
- Rosenberg, A., Saviane, I., Piotto, G., Aparicio, A., & Zaggia, S.R. 1998, *AJ*, 115, 648
- Rosenberg, A., Piotto, G., Saviane, I., & Aparicio, A. 2000a, *A&AS*, 144, 5
- Rosenberg, A., Aparicio, A., Saviane, I., & Piotto, G. 2000b, *A&AS*, 145, 451
- Sbordone, L., Bonifacio, P., Marconi, G., Buonanno, R., & Zaggia, S. 2005, *A&A*, 437, 905
- Schlegel, D.J., Finkbeiner, D.P., & Davis, M. 1998, *ApJ*, 500, 525
- Sirianni, M., Jee, M.J., Benitez, N., Blakeslee, J.P., Martel, A.R., Meurer, G., Clampin, M., De Marchi, G., Ford, H. C., Gilliland, R., and 4 coauthors 2005, *PASP*, 117, 1049
- Staneva, A., Spassova, N., Golev, V. 1996, *A&AS*, 116, 447
- Stetson, P.B., Hesser, J.E., Smith, G.H., Vandenberg, D.A., % Bolte, M. 1989, *AJ*, 97, 1360
- Van den Bergh, S. 2000, *The galaxies of the Local Group* (Cambridge: Cambridge University Press)
- Venn, K., Chutter, A., Irwin, M., Arimoto, N., Aoki, W., & Sadakane, K. 2007, *American Astronomical Society Meeting 210*, # 123.14
- Tautvaisienė, G., Wallerstein, G., Geisler, D., Gonzales, G., & Charbonnel, C. 2004, *AJ*, 127, 373
- Williams, B.F., & Hodge, P.W. 2001, *ApJ*, 548, 190
- Zinn, R.J. 1985, *ApJ*, 293, 424